

# Biomaterials Science

Accepted Manuscript

This article can be cited before page numbers have been issued, to do this please use: S. Font Tellado, J. A. Delgado, P. S.P. Poh, W. Zhang, M. García-Vallés, S. Martínez, A. Gorustovich, L. Morejón, M. van Griensven and E. Balmayor, *Biomater. Sci.*, 2021, DOI: 10.1039/D1BM01311D.



This is an Accepted Manuscript, which has been through the Royal Society of Chemistry peer review process and has been accepted for publication.

Accepted Manuscripts are published online shortly after acceptance, before technical editing, formatting and proof reading. Using this free service, authors can make their results available to the community, in citable form, before we publish the edited article. We will replace this Accepted Manuscript with the edited and formatted Advance Article as soon as it is available.

You can find more information about Accepted Manuscripts in the [Information for Authors](#).

Please note that technical editing may introduce minor changes to the text and/or graphics, which may alter content. The journal's standard [Terms & Conditions](#) and the [Ethical guidelines](#) still apply. In no event shall the Royal Society of Chemistry be held responsible for any errors or omissions in this Accepted Manuscript or any consequences arising from the use of any information it contains.

## ARTICLE

# Phosphorous pentoxide-free bioactive glass exhibits dose-dependent angiogenic and osteogenic capacities which are retained in glass polymeric composite scaffolds

Received 00th January 20xx,  
Accepted 00th January 20xx

DOI: 10.1039/x0xx00000x

Sonia Font Tellado,<sup>a</sup> José Angel Delgado,<sup>bc</sup> Su Ping Patrino Poh,<sup>ad</sup> Wen Zhang,<sup>ef</sup> Maite García-Vallés,<sup>g</sup> Salvador Martínez,<sup>g</sup> Alejandro Gorustovich,<sup>h</sup> Lizette Morejón,<sup>b</sup> Martijn van Griensven<sup>ai</sup> and Elizabeth Rosado Balmayor<sup>\*aj</sup>

Bioactive glasses (BGs) are attractive materials for bone tissue engineering because of their bioactivity and osteoinductivity. In this study, we report the synthesis of a novel phosphorous pentoxide-free, silicate-based bioactive glass (52S-BG) composed of 52.1% SiO<sub>2</sub>, 23.2% Na<sub>2</sub>O and 22.6% CaO (wt.%). The glass was thoroughly characterized. The biocompatibility and osteogenic properties of 52S-BG particles were analyzed *in vitro* with human adipose-derived mesenchymal stem cells (AdMSCs) and human osteoblasts. 52S-BG particles were biocompatible and induced mineralized matrix deposition and the expression of osteogenic markers (RunX2, alkaline phosphatase, osteocalcin, osteopontin, collagen I) and the angiogenic marker vascular endothelial growth factor (VEGF). Angiogenic properties were additionally confirmed in a zebrafish embryo model. 52S-BG was added to poly-ε-caprolactone (PCL) to obtain a composite with 10 wt.% glass content. Composite PCL/52S-BG scaffolds were fabricated by additive manufacturing and displayed high porosity (76%) and pore interconnectivity. The incorporation of 52S-BG particles increased the Young's modulus of PCL scaffolds from 180 to 230 MPa. AdMSC seeding efficiency and proliferation were higher in PCL/52S-BG compared to PCL scaffolds, indicating improved biocompatibility. Finally, 52S-BG incorporation improved the scaffolds' osteogenic and angiogenic properties by increasing mineral deposition and inducing relevant gene expression and VEGF protein secretion. Overall, 52S-BG particles and PCL/52S-BG composites may be attractive for diverse bone engineering applications requiring concomitant angiogenic properties.

## 1. Introduction

To date, a wide variety of biomaterials have been applied in bone tissue engineering. Among these, bioactive glasses (BGs) are particularly attractive because of their potential to induce bone formation (osteoinductivity) and ability to form a

hydroxycarbonate apatite layer on the glass surface when exposed to biological fluids (bioactivity).<sup>1</sup>

Since the commercialization of 45S5 Bioglass® (45% SiO<sub>2</sub>, 24.5% Na<sub>2</sub>O, 24.5% CaO and 6% P<sub>2</sub>O<sub>5</sub> in wt.%) in 1969,<sup>2</sup> a variety of BGs have been synthesized for bone regeneration. Commonly, silicon dioxide (SiO<sub>2</sub>), boron trioxide (B<sub>2</sub>O<sub>3</sub>) and/or phosphorous (P) form the main glass network, while elements such as sodium (Na), calcium (Ca), magnesium (Mg), strontium, (Sr) and also P can act as network modifiers, influencing the degree of solubility and the release of ionic products from BGs.<sup>3</sup> A large proportion of the currently available BGs are composed of silicon (Si) and P. It has been extensively reported that Si is essential for bone tissue formation and its calcification,<sup>4</sup> while P plays a role in stimulating matrix Gla protein expression, a key regulator in bone formation.<sup>5</sup> Interestingly, the role of phosphorous pentoxide (P<sub>2</sub>O<sub>5</sub>) remains strongly debated. P<sub>2</sub>O<sub>5</sub>-free BGs, that is, from the groups SiO<sub>2</sub>-CaO and SiO<sub>2</sub>-CaO-Na<sub>2</sub>O have shown to be highly advantageous.<sup>6-8</sup> These BGs have been shown to be bioactive<sup>6, 9, 10</sup> and capable of inducing extracellular matrix (ECM) secretion and mineralization by primary human osteoblasts (OBs).<sup>7</sup> In addition, P<sub>2</sub>O<sub>5</sub>-free BG may be particularly useful to some fabrication techniques.<sup>7</sup> Scaffolds with adequate mechanical properties and interconnected porosity have been produced using P<sub>2</sub>O<sub>5</sub>-free BG by foaming process techniques.<sup>7</sup> Overall, this suggests that

<sup>a</sup> Experimental Trauma Surgery, Klinikum rechts der Isar, Technical University of Munich, 81675 Munich, Germany.

<sup>b</sup> Center for Biomaterials, University of Havana, 10400 Havana, Cuba.

<sup>c</sup> Universitat Internacional de Catalunya, 08195 Barcelona, Spain.

<sup>d</sup> Berlin Institute of Health at Charité – Universitätsmedizin Berlin, Julius Wolff Institute, 13353 Berlin, Germany.

<sup>e</sup> Institute of Molecular Immunology and Experimental Oncology, Klinikum rechts der Isar, Technical University of Munich, 81675 Munich, Germany.

<sup>f</sup> Ethris GmbH, 82152 Planegg, Germany.

<sup>g</sup> Mineralogy, Petrology and Applied Geology Department, University of Barcelona, 08028 Barcelona, Spain.

<sup>h</sup> Interdisciplinary Materials Group-IESIING-UCASAL, INTECIN UBA-CONICET, A4400EDD Salta, Argentina.

<sup>i</sup> cBITE, MERLN Institute for Technology-Inspired Regenerative Medicine, Maastricht University, 6200 MD Maastricht, the Netherlands.

<sup>j</sup> IBE, MERLN Institute for Technology-Inspired Regenerative Medicine, Maastricht University, 6200 MD Maastricht, the Netherlands.

† Electronic Supplementary Information (ESI) available: Table S1 list the sequence for all primers used for qPCR. Table S2 shows the concentration (ppm) as detected by ICP-MS for Si and Ca released to the embryonic medium from the 52S-BG particles. Figure S1 shows Mcm5 and Bcl2 expression in human adipose-derived mesenchymal stem cells and human osteoblasts exposed to the 52S-BG particles. See DOI: 10.1039/x0xx00000x

P<sub>2</sub>O<sub>5</sub>-free BGs feature unique advantages while maintaining osteogenic properties. Furthermore, the presence of P<sub>2</sub>O<sub>5</sub> has been associated with a tendency for easy hydrolysis.<sup>11</sup> Therefore, P<sub>2</sub>O<sub>5</sub> BGs may be more suitable as temporary implants, highly attractive for soft tissue, rather than bone tissue engineering.<sup>11</sup>

Several studies have demonstrated that cell behavior, in particular osteogenesis, can be altered by the dissolution products of BGs (reviewed in <sup>3</sup>). Most investigation has been restricted to cell lines, resulting in the current lack of evidence in clinically relevant cells. Moreover, to date, there are limited studies which provide a direct comparison of the effects of BGs on different cell types relevant for bone tissue engineering, including human-derived mesenchymal stem cells and human OBs. Furthermore, most evidence on the angiogenic properties of these materials is described for Cu<sup>2+</sup> and Co<sup>2+</sup> doped glasses<sup>12, 13</sup> or for Boron-containing glasses.<sup>14</sup> Concerns exist regarding cellular toxicity of Co<sup>2+</sup> doped BGs.<sup>15, 16</sup> Despite their clear advantages, little evidence is available regarding the angiogenic properties of P<sub>2</sub>O<sub>5</sub>-free BGs.

The adoption of BGs for the regeneration of living bone in large volumes, load-bearing defects has been limited because of their inherent brittleness and low fracture toughness.<sup>17</sup> A good alternative is to use composite scaffolds to harness and combine the advantages of different biomaterials into a single component.<sup>18</sup> BGs are attractive additives that can be added to polymeric scaffolds to enhance the bioactivity of the final composite biomaterial.

In the present study, a novel P<sub>2</sub>O<sub>5</sub>-free BG containing 52.1% SiO<sub>2</sub>, 23.2% Na<sub>2</sub>O and 22.6% CaO (wt.%) was synthesized (termed 52S-BG hereafter). The dose-dependent biocompatibility and osteogenic and angiogenic potential of 52S-BG particles on human adipose-derived mesenchymal stromal cells (AdMSCs) and OBs were evaluated. In addition, the angiogenic potential of the 52S-BG particles was further investigated *in vivo* in a zebrafish embryo model. Subsequently, composite scaffolds comprising PCL and 10 wt.% 52S-BG particles were fabricated by melt-extrusion-based additive manufacturing. PCL is a biodegradable synthetic polymer with good rheological and viscoelastic properties that has been approved by the FDA in several biomedical devices.<sup>19, 20</sup> PCL is particularly attractive for tissue engineering. Its low melting temperature readily allows the fabrication of three-dimensional (3D) scaffolds using this polymer by various processing techniques.<sup>21</sup> However, PCL is hydrophobic and features poor bioactivity. We hypothesized that by fabricating a PCL/52S-BG composite scaffold, crucial features for tissue engineering would be gained. Therefore, the ability of PCL/52S-BG composite scaffolds to retain the bioactivity and osteogenic and angiogenic potential initially displayed by the 52S-BG particles was evaluated *in vitro* in AdMSCs.

## 2. Experimental

### 2.1. 52S-BG particles

**2.1.1. Precursor materials: Silica sand and calcite mineral.** The silica sand used as raw material for the synthesis of the glass

was extracted from the Santa Teresa silica sand deposit. This deposit is located in the southwest of Pinar del Rio province in Cuba; it is of alluvial origin and is characterized by quartzose sands. The silica sand used contained 99.2 wt.% SiO<sub>2</sub>.<sup>22</sup> The calcite mineral used during the glass synthesis was extracted from the Jaruco deposit in Mayabeque province in Cuba. The calcite mineral was composed of 57.62 ± 0.07 wt.% CaO, 0.269 ± 0.005 wt.% MgO, 0.25 ± 0.09 wt.% SiO<sub>2</sub> and trace elements.<sup>22</sup> Further characterization of the raw materials can be found elsewhere.<sup>22</sup> Prior to use, both materials were sieved and manually ground using an agate mortar.

**2.1.2. 52S-BG fabrication.** Glass synthesis was performed by melt quenching. Briefly, calcite mineral (source of calcium carbonate, CaCO<sub>3</sub>) and silica sand (source of silicon dioxide, SiO<sub>2</sub>) were mixed with sodium carbonate anhydrous (Na<sub>2</sub>CO<sub>3</sub>, 99.5%, AppliChem PanReac, Barcelona, Spain) in a molar proportion of 1:3:2, fused at 1400°C for 6 h and abruptly cooled to induce glass formation. Solid disc-shaped glass blocks were obtained. Subsequently, a powder was produced from the glass discs using a MM400 ball mill (Retsch GmbH, Haan, Germany) and particle size was characterized with a Zetasizer Nano 79 (Malvern Panalytical Ltd., Malvern, United Kingdom) using ethanol (96%) as a dispersion medium. The bioactive glass obtained is referred to as 52S-BG throughout this publication.

**2.1.3. 52S-BG characterization.** The elemental composition of synthesized 52S-BG was analyzed by X-ray fluorescence using a PW 2400 photometer (Philips, Cambridge, MA, USA) with two excitation sources, a rhodium anode and a golden anode. Identification of the glass crystalline phases was performed by X-ray diffraction (XRD) using a D5000 diffractometer (Siemens AG, Berlin, Germany) with CuK $\alpha$  radiation ( $\lambda = 1.5484 \text{ \AA}$ ) in the interval of 10–70° and an incident angle of 0.05°. Thermal analysis of the glass was performed using a NETZSCH STA 409 simultaneous thermogravimetric and differential thermal analyzer (TG-DTA, Netzsch GmbH, Selb, Germany). Aluminum oxide (Al<sub>2</sub>O<sub>3</sub>) in a static air atmosphere and a heating speed of 5°C/min was used as a reference material.

Analysis of 52S-BG bioactivity was performed by immersion in a simulated body fluid (SBF) solution prepared as described by Kokubo *et al.*<sup>23</sup> and used after sterile filtration. Samples were maintained in SBF for 15 days at 37°C and mineral deposition was analyzed with a JEOL JSM scanning electron microscope (SEM, JEOL Ltd., Tokyo, Japan) coupled with an Oxford LINK ISIS 300 (Oxford Instruments Ltd., High Wycombe, United Kingdom) energy dispersive X-ray (EDX) detector.

### 2.2. Fabrication of PCL and PCL/52S-BG scaffolds by additive manufacturing

52S-BG particles were incorporated into the PCL bulk. Briefly, 10% (w/v) PCL solution was prepared by dissolving 10 g PCL pellets (CAPA 6500, Perstorp Ltd., Warrington, United Kingdom) in 100 ml chloroform (MERCK Millipore, Melbourne, Australia) at room temperature. Subsequently, 10 wt.% 52S-BG particles (relative to the PCL mass) were added to the PCL solution and stirred to obtain a homogenous mixture. Given the small size of the 52S-BG particles, 10 wt.% was selected to prevent particle agglomeration that may compromise the scaffold mechanical properties.<sup>24, 25</sup> The PCL/52S-BG solution was precipitated into

5-fold excess ethanol (absolute, MERCK Millipore). The solid PCL/52S-BG composite was isolated and air-dried to evaporate the solvent. Finally, PCL and PCL/52S-BG scaffolds were fabricated using an in-house melt extrusion-based 3D printer at 90°C and 100°C, respectively.<sup>19</sup> All scaffolds were fabricated using a 21G nozzle with a lay-down pattern of 0–90°, filament gap of 1 mm and layer thickness of 0.4 mm. Scaffolds of 30 mm length (L) × 30 mm width (W) × 3 mm height (H) were fabricated. For cell culture, mechanical testing and degradation experiments, PCL and PCL/52S-BG scaffolds were cut in 4 mm (L) × 4 mm (W) × 3 mm (H) pieces. Subsequently, all scaffolds were immersed in 70% ethanol for 30 min under vacuum and treated with 5 M sodium hydroxide for 90 min at 37°C to increase surface roughness and expose the 52S-BG particles.<sup>19, 26</sup> Disinfection prior to cell culture was performed by treatment with 70% ethanol for 30 min.

### 2.3. Characterization of PCL and PCL/52S-BG scaffolds

Scaffold morphology, porosity, pore size distribution, filament thickness and 52S-BG particle content were analyzed by micro-computed tomography (Skyscan 1176, Bruker, Kontich, Belgium) at a voxel size of 9 μm (n = 6 for each scaffold type). Image reconstruction was performed using the Skyscan CTRecon software and image analysis was performed with the Skyscan CTAn software using a built-in algorithm.

Degradation and water uptake were analyzed in eight scaffolds of each type. For these experiments, the initial weight of each scaffold was recorded. Subsequently, each scaffold was placed in a 15 ml conical tube (Greiner Bio-One GmbH, Frickenhausen, Germany) and incubated at 37°C with 3 ml phosphate-buffered saline (PBS) solution for 2 or 4 weeks. After each time point, the scaffolds were collected from the PBS and weighted twice, *i*) immediately after removing the excess PBS and *ii*) 48 h after vacuum-drying (final, constant weight). Water uptake and weight loss were calculated using previously reported equations.<sup>27</sup>

The mechanical properties of the PCL and PCL/52S-BG scaffolds (n = 8 for each type of scaffold) were tested by subjecting the scaffolds to 10% compression using a zwickLine 1120 microtester (ZwickRoell GmbH, Ulm, Germany) fitted with a 2.5 kN load cell at a rate of 1 mm/min. Young's modulus was calculated from the stress-strain curve at values between 3–8% strain. The area of the scaffolds was calculated as (L) × (H) × (100 – % porosity). Scaffolds were tested before and after 2 or 4 weeks of degradation in PBS.

### 2.4. Ion release from 52S-BG particles and PCL/52S-BG scaffolds

52S-BG particles (concentrations of 100, 200, 300, 400 and 1000 μg/ml) and PCL and PCL/52S-BG scaffolds were incubated with non-supplemented low glucose Dulbecco's Modified Eagle Medium (DMEM) at 37°C. The pH was measured using a WTW inoLab 720 pH meter (Gemini B.V., Apeldoorn, the Netherlands) immediately and after 3 or 7 days of incubation. The cumulative release of Si, Na, Ca and P ions was analyzed by inductively coupled plasma optical emission spectrometry (ICP-OES, Optima 8300, PerkinElmer, Waltham, MA, USA). ICP-OES measurements were performed on the supernatants collected at 3, 6 and 12 h and 1, 5 and 7 days after incubation. The data of ionic concentration was normalized to the DMEM ionic

concentration that was measured as baseline control at each time-point.

DOI: 10.1039/D1BM01311D

### 2.5. Cell isolation and expansion

Tissue collection for cell isolation was approved by the local ethical committee of the "Klinikum rechts der Isar" at the Technical University of Munich (Munich, Germany). Tissue collection was performed after obtaining the patient's written informed consent and in accordance with the most recent guidelines of the declaration of Helsinki. Six healthy human donors were enrolled in this study. Adipose tissue from subcutaneous fat (n = 3) was used for AdMSCs while bone tissue from femoral heads (n = 3) was collected for OBs isolation.

AdMSCs were isolated following the protocol described in <sup>28</sup>. Briefly, fat tissue was cut into small pieces (0.5–2 mm), washed twice in PBS and centrifuged (5810R, Eppendorf AG, Hamburg, Germany) at 600 g for 10 min. Subsequently, the tissue was digested with 1.45% collagenase solution (Biochrom GmbH, Berlin, Germany) for 30 min at 37°C and centrifuged at 600 g for 10 min to obtain a cell pellet. Cells were cultured and expanded on 175 cm<sup>2</sup> flasks (Eppendorf AG) using AdMSC expansion medium (i.e. high glucose DMEM supplemented with 10% fetal bovine serum (FBS) and 1% penicillin-streptomycin (P/S)) at 37°C under 5% CO<sub>2</sub>. The culture medium was changed 24 h after isolation and twice a week during expansion.

OBs were isolated following the protocol described in <sup>29</sup>. In brief, cancellous bone was cracked in small pieces (1–4 mm) and washed twice with PBS. Subsequently, bone pieces were transferred to 175 cm<sup>2</sup> flasks (Eppendorf AG) and cultured in OB expansion medium (i.e. low glucose DMEM supplemented with 10% FBS, 1% P/S and 0.2 M L-ascorbate-2-phosphate) at 37°C under 5% CO<sub>2</sub>. The cell culture medium was changed twice a week, passaging the cells once 80% confluence was reached.

### 2.6. Cell culture with 52S-BG particles

AdMSCs or OBs were seeded on tissue culture plates (TPP Techno Plastic Products AG, Trasadingen, Switzerland) at a density of 2.1 × 10<sup>4</sup> cells/cm<sup>2</sup>. Subsequently, both cell types were independently cultured in the presence of different 52S-BG particle concentrations (direct contact with the particles; 100–1000 μg/ml, table 1).

For cytotoxicity and cell proliferation assays, expansion medium was used according the cell type investigated. For ALP activity, mineralization and gene/protein expression assays, cells were cultured under serum starvation conditions (i.e. low glucose DMEM + 2% FBS + 1% P/S) to support *in vitro* cellular differentiation. Low serum conditions have been correlated with a better maintenance of MSCs pluripotent phenotype <sup>30</sup> as well as their superior angiogenic <sup>31</sup> and osteogenic differentiation.<sup>32</sup> A plausible explanation for this may be related to the low serum levels present at poorly vascularized injuries and bone fracture sites. Therefore, low serum conditions may be more accurately mimicking the bone fracture microenvironment. Additionally, serum starvation medium was supplemented with 10 mM β-glycerophosphate (AppliChem GmbH, Darmstadt, Germany) and 0.2 M L-ascorbate-2-phosphate to support *in vitro* matrix deposition.<sup>33</sup> An overview of the setup of the cell culture experiments used during the 52S-

BG particles evaluation is presented in table 1. Medium change was performed twice a week.

### 2.7. Cell culture on PCL and PCL/52S-BG scaffolds

AdMSCs were seeded on PCL and PCL/52S-BG scaffolds at a density of  $2 \times 10^4$  cells/scaffold. In samples for gene and protein expression experiments, cell density was increased to  $2 \times 10^5$  cells/scaffold to obtain enough cellular material for these assays. Scaffolds were placed in 48-well plates and seeded by using 30  $\mu$ L cell suspension/scaffold. After 1.5 h of incubation at 37°C under 5% CO<sub>2</sub>, fresh culture medium was added to reach a final volume of 1 ml. Culture was performed at 37°C under 5% CO<sub>2</sub> (further details are listed in table 1). Medium was changed twice a week.

### 2.8. Biocompatibility of 52S-BG particles and PCL/52S-BG scaffolds: Cell viability and proliferation

Live/dead staining was performed of AdMSCs and OBs after separate culture with 52S-BG particles. In addition, AdMSCs cultured on PCL or PCL/52S-BG scaffolds were also evaluated. The times of observation selected were 1, 3 and 7 days after culture (for both, particles and scaffolds). For this experiment, samples were washed with PBS and incubated for 15 min at 37°C with a solution containing 0.05% calcein AM, 0.2% propidium iodide and 0.01% Hoechst (all solutions prepared in sterile PBS). Images were obtained using a B7-9000 fluorescence microscope (Keyence, Osaka, Japan) and processed using the BZ-II Analyzer software.

For cytotoxicity, the MTT (3-(4,5-dimethylthiazol-2-yl)-2,5-diphenyltetrazolium bromide) assay was performed to evaluate both particles and scaffolds, while the lactate dehydrogenase (LDH) assay was additionally performed for the scaffolds.

**2.8.1. MTT assay.** Following the selected times of observation of 1, 3 or 7 days after culture, samples were washed with PBS and incubated in MTT solution (1.2 mM in PBS, Carl Roth GmbH, Karlsruhe, Germany) for 1.5 h at 37°C. Subsequently, samples were incubated for either 10 min (AdMSCs or OBs cultured with 52S-BG particles) or 30 min (AdMSCs cultured on PCL or PCL/52S-BG scaffolds) in a solution containing 10% sodium dodecyl sulfate and 0.6% acetic acid in dimethylsulfoxide (Carl Roth GmbH) at room temperature. Absorbance at 570 nm and 690 nm was determined using a FLUOstar Omega plate reader photometer (Labtech, Ortenberg, Germany). Latex rubber was used to induce cell death (MTT positive control).<sup>34</sup> Untreated cells were used as 100% cell viability (MTT negative control). With the scaffolds, the results were reported as optical density from PCL/52S-BG scaffolds compared to PCL scaffolds used as the control.

**2.8.2. LDH assay.** This assay was performed to evaluate the activity of LDH, a stable cytoplasmic enzyme, in the cell culture supernatants after culture of AdMSCs on the PCL/52S-BG scaffolds. This enzyme is only released to the extracellular environment by damaged cells.<sup>35</sup> For LDH determination, AdMSCs were cultured on PCL/52S-BG scaffolds for 1, 3 or 7 days. Similar to the MTT assay, PCL scaffolds were used as the control. The assay was conducted by means of a Fluitest LDH-L kit (Analyticon Biotechnologies AG, Lichtenfels, Germany) following the manufacturer's instructions. Briefly, at the predetermined observation times, 100  $\mu$ L cell culture

supernatant were transferred in triplicate to a 96-well plate and 100  $\mu$ L LDH working solution were applied on top. Rapidly after addition, absorbance was determined at 340 nm using the plate reader. The LDH concentration was calculated by means of a calibration curve using an LDH standard provided in the Fluitest LDH-L kit.

**2.8.3. DNA quantification assay.** Cell proliferation was evaluated by means of the total DNA amount, as determined using a Quant-iT™ PicoGreen dsDNA assay kit (Thermo Fisher Scientific, Waltham, MA, USA) following the manufacturer's instructions. Briefly, 3, 7 or 14 days after AdMSCs or OBs were cultured in contact with the 52S-BG particles, the cells were thoroughly washed twice with PBS. Subsequently, the cells were vigorously resuspended with 500  $\mu$ L ultra-pure dH<sub>2</sub>O (Aqua, B. Braun, Melsungen, Germany). Cell lysates were obtained by cycles of freeze/thawing. For the assay, equal volumes of cell lysate and Quant-iT Pico-Green working solution were pipetted into a 96-well plate. The plates were incubated for 5 min at 37°C. Thereafter, fluorescence was determined (emission: 520 nm and excitation: 485 nm) in the plate reader. The DNA concentrations were calculated using a calibration curve.

### 2.9. ALP activity

ALP activity was evaluated as a first indication of osteogenic differentiation. In brief, 1, 3, 7 or 14 days after culture of AdMSCs or OBs with the 52S-BG particles, cells were washed twice with PBS and incubated with ALP substrate solution. This solution consisted of 3.4 mM pNpp (4-nitrophenyl phosphate di-sodium salt hexahydrate) prepared in a basic buffer. Cells were incubated with the ALP substrate solution for 30 min at 37°C and the absorbance was determined at 405 nm using the plate reader.

### 2.10. Mineralization

**2.10.1. AdMSCs cultured with 52S-BG particles.** Analysis of matrix mineralization was performed by Alizarin Red S staining. For this, AdMSCs were cultured with 100  $\mu$ g/ml or 300  $\mu$ g/ml 52S-BG particles (table 1). The experimental conditions used for the cell culture are summarized in table 1. At predetermined observation times of 14, 21 or 35 days after culture, cells were carefully washed with PBS to remove glass particles. Particular care was taken to ensure complete BG particle removal to prevent their reaction with the Alizarin Red S dye. Subsequently, the cells were fixed with 96% ethanol for 30 min at 4°C, washed with dH<sub>2</sub>O and stained with 0.5% Alizarin Red S solution for 10 min at room temperature. Images were obtained with the Keyence B7-9000 microscope. For quantification, Alizarin Red S dye was extracted from the cell layer by adding 10% hexadecylpyridiniumchloride and subsequently incubating for 15 min at room temperature. The absorbance was determined at 405 nm using the plate reader.

**2.10.2. AdMSCs cultured on PCL/52S-BG scaffolds.** von Kossa staining was performed 14, 21 or 35 days after AdMSC culture on PCL or PCL/52S-BG scaffolds. For this, cells-seeded scaffolds were incubated in ice cold methanol (Carl Roth GmbH) for 15 min and thereafter in 3% silver nitrate solution (MERCK Millipore) for 30 min at room temperature. Subsequently, samples were washed with dH<sub>2</sub>O and incubated in 1% pyrogallol solution (Carl Roth GmbH) for 3 min. Sample fixation was

performed by incubating the samples in 5% sodium thiosulfate solution (MERCK Millipore) for 5 min and in 96% ethanol for 1 min. Images were obtained with the Keyence B7-9000 microscope.

Electron microscopy using a SEM/EDX was performed after 35 days of culture. Samples were dehydrated by sequential immersion in 30%, 45%, 70%, 85% and 100% ethanol solutions (2 × 15 min) followed by treatment with hexamethyldisilazane (3 × 10 min) and air dried overnight. In this case, a JEOL J-7100F field emission SEM (JEOL Ltd.) was used. The equipment was coupled to an EDX detector Inca 250 (Oxford Instruments Ltd.) and backscattered electron detector. The samples were analyzed using an acceleration voltage of 20kV. The samples were coated with carbon to improve their conductivity.

### 2.11. Gene expression

Gene expression analysis was performed to evaluate cellular events such as *i*) proliferation (Cyclin D1 and minichromosome maintenance complex 5 (Mcm5), *ii*) apoptosis (B-cell lymphoma 2 (Bcl2) and caspase 3), *iii*) osteogenesis (Runt-related transcription factor 2 (RunX2), ALP, osteocalcin and osteopontin), *iv*) ECM secretion (collagen I) and *v*) vascularization (vascular endothelial growth factor (VEGF)). The primers used (Eurofins, Planegg, Germany) are listed in the supplementary table S1.

AdMSCs and OBs cultured with either 100 µg/ml or 300 µg/ml 52S-BG particles were used for gene expression analysis. Cells cultured without 52S-BG particles but under the same conditions were used as controls. Moreover, AdMSCs were additionally cultured on the PCL/52S-BG scaffolds, using PCL scaffolds without glass content for comparison. During these experiments, serum starvation medium was used as indicated in table 1.

At the predetermined observation times of 3, 7 or 14 days after culture, the culture media was removed and the cell monolayer (52S-BG particles culture) and cell-seeded scaffold were thoroughly washed with PBS. Subsequently, RNA isolation reagent (TRI reagent®, MERCK Millipore) was added to each well plate (500 µL/well for the particles or 150 µL/scaffold). Cell lysis was performed by a freeze/thawing cycle in TRI reagent®. For cells cultured with the 52S-BG particles, the cellular material was collected using a cell scraper (Sarstedt AG, Nümbrecht, Germany). For cell-seeded scaffolds, the samples were briefly vortexed to ensure the collection of all cellular material. RNA isolation was performed using a standard chloroform extraction protocol followed by ethanol precipitation. RNA was quantified using a Biophotometer (Eppendorf AG) by determining the absorbance at 280 nm. Purity was determined by the 260/280 nm and 260/230 nm ratios. RNA was retro-transcribed to cDNA immediately after isolation with the first strand cDNA synthesis kit (Thermo Fisher Scientific) following the manufacturer's instructions and using as the thermocycler a C1000 Touch Thermal Cycler (Eppendorf AG). The obtained cDNA was diluted in ultrapure, PCR grade ddH<sub>2</sub>O (Carl Roth GmbH) to a final concentration of 10 ng/µL.

Quantification of gene expression was performed by real-time quantitative polymerase chain reaction (qPCR) using 30 ng cDNA template and SsoFast EvaGreen supermix (Bio-Rad

Laboratories Inc., Hercules, CA, USA) in a CFX96 Real Time System (Bio-Rad Laboratories Inc.). The thermal profile consisted of an initial denaturation cycle (3 min at 95°C) followed by 40 cycles of short denaturation (40 s at 95°C) and annealing/extension (10 s at 60°C).

For the cells cultured with 52S-BG particles, the target C<sub>t</sub> values were subtracted from the C<sub>t</sub> values of the housekeeper (β-tubulin) to obtain the dC<sub>t</sub> values. The dC<sub>t</sub> values from the control samples, that is, cells cultured without the BG particles, were subtracted from the correspondent experimental groups to obtain ddC<sub>t</sub> values, which were expressed as 2<sup>-ddC<sub>t</sub></sup>. For the cells cultured on the scaffold, dC<sub>t</sub> values were calculated and expressed as 2<sup>-dC<sub>t</sub></sup>.

### 2.12. VEGF protein secretion and total protein quantification

The supernatants corresponding to AdMSCs cultured with either 52S-BG particles or PCL/52S-BG scaffolds were collected at 3, 7 or 14 days after culture for total protein and VEGF quantification. Total protein content was quantified by the Lowry assay using bovine serum albumin as the standard. Briefly, samples and standards were incubated for 10 min at room temperature with a solution containing 0.02% di-sodium tartrate (MERCK Millipore) and 0.01% CuSO<sub>4</sub>. This was followed by a 1.5 h incubation with 0.4 g/ml Folin's reagent. The protein concentration was calculated by determining the absorbance at 750 nm in the plate reader. The amount of VEGF secreted to the cell culture media was analyzed by enzyme-linked immunosorbent assay using the human VEGF Quantikine ELISA kit (R&D Systems Inc., Minneapolis, MN, USA) following the manufacturer's instructions. The total protein content in each sample was used to normalize the VEGF content between samples.

### 2.13. Angiogenesis induced by 52S-BG particles in vivo: Zebrafish embryo model

To obtain the ionic dissolution products from the 52S-BG particles, 10% (w/v) of particles were incubated in embryonic medium at 37°C in an orbital shaker for 3 or 7 days. Following centrifugation, the samples were filtered with a 0.2 µm cellulose acetate membrane and adjusted to pH 7. The embryonic medium used in these experiments was prepared from a stock salt solution (40 g Instant Ocean® Salt, Blacksburg, VA, USA) in dH<sub>2</sub>O by reverse osmosis to a final concentration of 60 µg/ml (pH 7). The soluble Si and Ca ions leached from the 52S-BG particles were determined by inductively coupled plasma mass spectrometry.

A zebrafish (*Danio rerio*) breeding colony (wild-type AB strain) provided by N. Calcaterra (IBR-CONICET, Rosario, Argentina) were maintained at the Zebrafish Facilities of the National University of Salta, Argentina. Zebrafish embryos, 48 h post-fertilization (hpf) and previously dechorionated and depigmented were used. Depigmentation was performed at 24 hpf with 0.2 mM 1-phenyl-2-thiourea. Embryos were incubated in six-well plates at 28.5°C for 24 h. The working volume used was 5 ml per well. Study samples were: plain embryonic medium (negative control), embryonic medium containing the ionic dissolution products from the 52S-BG particles and embryonic medium supplemented with 10 µg/ml basic fibroblast growth factor (bFGF, positive control). Thirty (n = 30)

embryos were used per treatment and each experiment was performed twice ( $n = 2$ ). Once the observation time of 24 h was reached, the embryos were anesthetized with tricaine, fixed in paraformaldehyde at 4% for 1 h at room temperature and processed to subsequently analyze the subintestinal vascular plexus by enzyme-histochemical identification of endogenous alkaline phosphatase, following the protocol described by Kamei *et al.*<sup>36</sup> Images were obtained using the digital microscope Keyence VHX-900F (scans) and the Keyence B7-9000 fluorescent microscope (10 $\times$  magnification). Semi-quantification of the sub-intestinal vein (SIV) was performed using the imaging analysis software Fiji for Image J (National Institutes of Health, Bethesda, MD, USA). The SIV space delimited by veins below the same five somites was selected to calculate the SIV area. The length of the SIV basket was also determined by considering the distance between the posterior cardinal vein and the bottom end of the SIV. Additionally, the number of compartments per SIV was also calculated.

#### 2.14. Statistical analysis

Cell culture experiments reported in this study were performed using triplicate samples or more. Each experiment was independently repeated at least twice. Three different human donors were used per tissue type. For the zebrafish experiments, 30 embryos per group was used in two independent experiments. Therefore, 60 individual samples were considered per analyzed group.

Statistical analysis was performed with GraphPad prism 9.0.0 (GraphPad software, San Diego, CA, USA). Data was analyzed by one-way ANOVA and Tukey's correction (Gaussian distribution) or Kruskal-Wallis and Dunn's correction (non-Gaussian distribution). When only two data sets were compared, data was analyzed with the two-tailed Student T test. Values were considered significant at  $p < 0.05$ . The  $p$  values were reported following GraphPad recommendations (i.e. \*  $p < 0.05$ , \*\*  $p < 0.01$ , \*\*\*  $p < 0.001$ , \*\*\*\*  $p < 0.0001$ ).

### 3. Results

#### 3.1. Physical and chemical characterization of synthesized 52S-BG

A new type of bioactive glass was obtained using silica sand and calcite mineral as precursor materials. The obtained glass, termed 52S-BG, was rich in silica and free of  $P_2O_5$ . Its chemical composition is shown in table 2. The main oxides that form the glass were  $SiO_2$  ( $52.1 \pm 0.3$  wt.%),  $Na_2O$  ( $23.2 \pm 0.1$  wt.%) and  $CaO$  ( $22.6 \pm 0.5$  wt.%). Other elements, including  $Al_2O_3$  and  $MgO$ , were present in small amounts and represented in total  $\leq 0.61$  wt.% of the total mass. Negligible  $P_2O_5$  content ( $\leq 0.027$  wt.%) was detected. XRD analysis showed the presence of a broad band at  $32^\circ$  (figure 1A), known to be present in amorphous materials. Unexpectedly, few peaks appeared in the diffractogram, which may indicate the presence of crystalline phases. This might be related to the presence of trace elements within the glass that could be responsible for inducing the crystallization of some silicate phases.<sup>22, 37</sup> Thermal analysis performed by TG-DTA showed a total mass loss of  $< 1\%$  upon heating (figure 1B), which can be explained by water loss at  $82^\circ C$

( $\alpha$ ) and  $-OH$  group breakage at  $174^\circ C$  ( $\beta$ ). Moreover, an endothermic transformation was observed at  $564^\circ C$  ( $\gamma$ ) caused by glass transition ( $T_g$ ), followed by an exothermic transformation between  $680-690^\circ C$  ( $\delta$ ) caused by glass crystallization ( $T_c$ ). Finally, melting occurred at  $1282^\circ C$  ( $\epsilon$ ), which corresponded to glass fusion ( $T_m$ ).

#### 3.2. In vitro bioactivity of 52S-BG: Dissolution ionic products

An *in vitro* incubation in SBF was performed to evaluate 52S-BG bioactivity. Two weeks post incubation, mineral deposition could be observed on the glass surface (SEM, figure 1C). The deposited mineral layer resembled a dense apatite-like layer. At higher magnification (insert in figure 1C), a cauliflower-like morphology of a dimension in the order of few micrometers was observed. This morphology is typically observed on bioactive materials as a reaction to SBF immersion. A representative EDX spectrum (figure 1C) indicated that the mineral deposits were composed of calcium (Ca) and phosphate (P).

A fine 52S-BG powder was produced from the obtained glass discs by mechanical milling. Over 90% of these 52S-BG particles were characterized by a size of  $372.7 \pm 31.2$  nm. Incubation of these particles in cell culture media resulted in a rapid pH increase (first 30 min), which occurred in a concentration-dependent manner (figure 1D). It was noted that after 3 and 7 days of incubation the pH stabilized to values of 7.6–8 for all the tested conditions, comparable to that of the control (cell culture media alone). The concentration of relevant ions (i.e. Si, Na, Ca and P) was analyzed after incubating different amounts of 52S-BG particles in cell culture media. The release curves are shown in figure 1E. Overall, a dependency was observed between the concentration of ions released into the media and the number of particles incubated. In the case of Si, this ion was detected in the range of 3–48 ppm and its concentration increased proportionally to the 52S-BG concentration. Most of the Si release occurred during the first 24 h of incubation, indicating a burst-like release. For the lower 52S-BG concentrations tested, Si peaked at approximately 24 h after incubation. Increasing the 52S-BG concentration to 1000  $\mu g/ml$  resulted in a steady increase of Si levels, with no peak reached up to 7 days post-incubation. Na, Ca and P release displayed different patterns from Si. Na levels initially increased for all samples containing  $\geq 200$   $\mu g/ml$ . Interestingly, in the sample containing the low 52S-BG particle concentration of 100  $\mu g/ml$ , an initial reduction of the Na concentration was observed to below that present in plain cell culture medium. This indicated a Na uptake from the medium by the glass particles. At the end of the observation period of 7 days, Na levels were in the range 136–295 ppm when considering all the evaluated samples. Ca and P levels displayed very similar patterns that were specific for each glass concentration. Interestingly, these two ions showed a decrease with the incubation time. This may indicate that an uptake of Ca and P by the glass particles occurred during the incubation in cell culture medium.

#### 3.3. Cytotoxicity and proliferation of AdMSCs and OBs in contact with 52S-BG particles

The cytotoxicity of 52S-BG particles was tested *in vitro* using human AdMSCs and OBs with a range of particle concentrations

of 100–1000  $\mu\text{g/ml}$  (figure 2A and B). The highest concentration of 1000  $\mu\text{g/ml}$  particles resulted in significant cytotoxicity for both cell types at all the evaluated observation times ( $p < 0.001$ ). Interestingly, the 52S-BG particles impacted the metabolic activity of AdMSCs and OBs in a dose-dependent manner. A concentration of 52S-BG particles of  $\leq 400 \mu\text{g/ml}$  resulted in high biocompatibility on AdMSCs while OBs appeared to be more susceptible to cell death when exposed to a high glass particle concentration. Metabolically active AdMSCs significantly increased proportionally to the glass concentration ( $p < 0.001$ ) at day 7 compared to that of days 1 and 3 after culture. By contrast, the metabolic activity of OBs tended to decrease with increasing 52S-BG particle concentration for up to 3 days (figure 2B). For the culture containing 400  $\mu\text{g/ml}$  52S-BG particles, OB metabolic activity was approximately 70% compared to the control ( $p < 0.05$ ), indicating slight toxicity. However, after 7 days of culture, the OB metabolic activity was restored to levels similar to the 100% viability control. Concentrations of 200 and 300  $\mu\text{g/ml}$  52S-BG particles resulted in a significant increase in metabolically active OBs after 7 days of culture ( $p < 0.05$ ). These results agree with the live/dead staining (figure 2C), showing that after 7 days of culture with 52S-BG particles at concentrations up to 400  $\mu\text{g/ml}$ , the majority of AdMSCs and OBs were alive and apoptotic cells were almost undetectable. In the 1000  $\mu\text{g/ml}$  52S-BG particles culture groups, no cells were detectable, indicating that all the cells had died and detached from the plate. Interestingly, the cell organization was greatly impacted by the presence of the glass particles. This was particularly observed for AdMSCs, where flower-like cellular clusters were formed that were more pronounced in the presence of a higher particle concentration (figure 2C, upper row).

The influence of 52S-BG particles on AdMSC and OB proliferation was also evaluated. 52S-BG particles at concentrations up to 400  $\mu\text{g/ml}$  supported AdMSC proliferation over time and was concentration-dependent (figure 2D). In particular, the proliferation rate of AdMSCs cultured with 400  $\mu\text{g/ml}$  52S-BG particles increased significantly between 3 and 7 days of culture ( $p < 0.05$ ). A similar proliferative behavior was observed for OBs (figure 2E). In this case, however, it was noted that 400  $\mu\text{g/ml}$  52S-BG particles did not appear to stimulate OB proliferation. Indeed, OB proliferation when in contact with 400  $\mu\text{g/ml}$  particles was significantly lower than that when cultured with lower concentrations of 52S-BG particles ( $p < 0.05$ ). Little or no dsDNA was detected in the 1000  $\mu\text{g/ml}$  culture conditions for both AdMSCs and OBs (figure 2D and E).

### 3.4. Effect of 52S-BG particles on ALP activity of AdMSCs and OBs

To evaluate whether the newly developed glass formulation could stimulate osteogenesis *in vitro*, we first evaluated its effect on ALP activity of both cell types. Because 1000  $\mu\text{g/ml}$  displayed cytotoxicity towards the cells, we excluded this concentration in further tests.

When cultured under serum starvation and no additional supplementation, both AdMSCs and OBs displayed decreased ALP activity with increasing 52S-BG concentration (figure 3A and C). OBs after 14 days of culture with the different glass

particle concentrations displayed very similar ALP activity results and no decrease of the activity values was detected. In the presence of 300  $\mu\text{g/ml}$  52S-BG particles,  $\beta$ -glycerophosphate and L-ascorbate-2-phosphate, AdMSCs clearly displayed increased ALP activity with time (figure 3B), which was statistically significant at 14 days post-culture compared to control ( $p < 0.05$ ). By contrast, ALP activity of OBs decreased with increasing 52S-BG concentration up to 7 days of *in vitro* culture (figure 3D). On the basis of these results, 52S-BG particles in concentrations of 100  $\mu\text{g/ml}$  and 300  $\mu\text{g/ml}$  were selected to further study the osteogenic effect of this material.

### 3.5. Mineralized matrix deposition by AdMSCs in contact with 52S-BG particles

A positive effect on mineral deposition by AdMSCs was observed upon culturing these cells with 300  $\mu\text{g/ml}$  52S-BG particles (figure 3E). At 35 days post-stimulation, ample mineralized matrix was observed. 52S-BG particles in culture medium without cells showed no background staining (figure 3E, material control). Colorimetric quantification of Alizarin Red S dye after extraction supported the qualitative observations (figure 3F). Matrix mineralization was significantly higher for AdMSCs in the presence of 300  $\mu\text{g/ml}$  52S-BG particles ( $p < 0.05$ , 35 days). Moreover, a synergistic action was observed, where  $\beta$ -glycerophosphate and L-ascorbate-2-phosphate appeared to be crucial for *in vitro* mineralization induced by the 52S-BG particles. AdMSCs that were solely stimulated with  $\beta$ -glycerophosphate and L-ascorbate-2-phosphate, that is, in the absence of 52S-BG particles, did not display mineralization (figure 3E, upper row).

SEM/EDX analysis of the mineral nodules found in the 300  $\mu\text{g/ml}$  group confirmed that the deposited mineral consisted of calcium and phosphate (figure 3G).

### 3.6. Effect of 52S-BG particles on AdMSC and OB gene expression

The expression of the proliferation marker Cyclin D1 was increased by both cell types after 3 days of culture in the presence of 52S-BG (figure 4A and B). This effect was particularly clear when cells were cultured with 300  $\mu\text{g/ml}$  52S-BG particles, with both cell types showing a 2-fold increase in Cyclin D1 expression, although not statistically significant ( $p > 0.05$ ). Cyclin D1 expression upregulation was supported by an upregulation of *Mcm5* in AdMSCs after 3 days of culture with 300  $\mu\text{g/ml}$  52S-BG (supplemental figure S1A). Of note, at the later time of observation of 14 days, a significant upregulation of 4-fold ( $p < 0.05$ ) of Cyclin D1 expression was observed for OB cultures with 300  $\mu\text{g/ml}$  52S-BG (figure 4B). This may indicate a positive effect of the 52S-BG particles on OB proliferation. However, the analysis of OB *Mcm5* gene expression showed a negligible effect of the particles on its expression (supplemental figure S1B).

With respect to apoptosis, no significant changes in the gene expression of the pro-apoptotic marker *Casp3* was found in either cell type or the conditions evaluated (figure 4A and B). Furthermore, no significant effect of 52S-BG was detected on AdMSC expression of the anti-apoptotic marker *Bcl2* (supplemental figure S1C). Interestingly, OBs cultured for 14



days with 300  $\mu\text{g}/\text{ml}$  52S-BG particles displayed upregulated Bcl2 expression ( $p > 0.05$ , supplemental figure S1D).

Subsequently, the gene expression patterns of the osteogenic markers RunX2, ALP, osteocalcin, osteopontin and collagen type I were evaluated. The results are shown in figure 4C, E and G for AdMSCs and figure 4D, F and H for OBs. Cell culture with 52S-BG slightly stimulated the expression of the early osteogenic marker RunX2 (figure 4C and D). This was more pronounced for OBs (figure 4D), which showed an upregulation of RunX2 for both 52S-BG concentrations tested. An ALP upregulation was also observed for both cell types. After 14 days of culture with 300  $\mu\text{g}/\text{ml}$  52S-BG, ALP was significantly upregulated ( $p < 0.05$  for AdMSC, figure 4C and  $p < 0.0001$  for OBs, figure 4D). Interestingly, the lower 52S-BG particle concentration tested (i.e. 100  $\mu\text{g}/\text{ml}$ ) stimulated early ALP expression (7 days after culture) in AdMSCs. This might indicate that concentrations  $< 300 \mu\text{g}/\text{ml}$  52S-BG are required when early ALP expression is desired in AdMSCs cultures, possibly due to a more efficient cellular uptake of released ions from the glass particles. The late osteogenesis marker osteocalcin displayed significant upregulation only in OBs cultured with 300  $\mu\text{g}/\text{ml}$  52S-BG particles (4-fold,  $p < 0.01$ , figure 4F). Notably, osteopontin expression was significantly upregulated in AdMSCs (5- to 10-fold,  $p < 0.05$ ) and OBs (10- to 30-fold,  $p < 0.05$ ) with 300  $\mu\text{g}/\text{ml}$  52S-BG particles (figure 4E and F). The expression pattern of osteopontin with time of the *in vitro* culture was similar for both cell types cultured with the glass particles. Collagen type I expression, as an indication of matrix deposition, was also evaluated. Similar to osteocalcin, this marker displayed significant upregulation only for OBs cultured with 300  $\mu\text{g}/\text{ml}$  52S-BG particles (9-fold,  $p < 0.0001$ , figure 4H), but in this case at a later time of culture.

### 3.7. Effect of 52S-BG particles on angiogenesis: gene expression and protein secretion

To gain an insight into the angiogenic properties of the newly developed 52S-BG, VEGF expression and protein production were evaluated. AdMSC and OB cultures followed a similar 52S-BG dose-dependent VEGF expression pattern. VEGF gene expression was upregulated after 3 days of AdMSC (2.5-fold) and OB (6-fold,  $p < 0.001$ ) culture with 300  $\mu\text{g}/\text{ml}$  52S-BG particles (figure 5A). Thereafter, VEGF expression decreased to control levels. However, at a later culture time (i.e. 14 days), VEGF expression slightly increased again for the higher concentration of glass particles (300  $\mu\text{g}/\text{ml}$ ). In addition to gene expression analysis, VEGF protein secretion was evaluated in AdMSCs (figure 5B). Cells cultured in the presence of the glass displayed an overall lower protein production in comparison to control cells. Despite this, VEGF production steadily increased in the presence of the glass particles over time ( $p = 0.0001$ ), while the control cells appeared to reach a plateau between 7 and 14 days of culture. VEGF production by AdMSCs on 52S-BG stimulation appeared to be initiated at late times after *in vitro* stimulation.

### 3.8. Effect of 52S-BG particles on *in vivo* angiogenesis

The subintestinal plexus or “vascular bed” of the developing fish embryo is ideal to investigate the early stages of organ-specific vessel formation. It comprises the suprainstestinal artery, SIV

and interconnecting vessels. In our study, zebrafish embryos incubated with solutions containing released glass ions (supplementary table S2) displayed vessel formation similar to that observed in the positive, growth factor control (figure 5D, E). By contrast, a stereotypical basket-shaped structure formation was observed in the negative controls (i.e. zebrafish embryo grown in standard media, figure 5C). The semi-quantification at the SIV region for the 52S-BG-treated groups showed an increase in the SIV area similar to that of the bFGF-positive control group (figure 5F). At 24 h post exposure, no significant difference in the SIV area was found between the 7-day 52S-BG ionic dissolution product group and the bFGF positive control ( $p = 0.42$ ). Moreover, the number of compartments and vascular loops formed were also greater for the 52S-BG-treated embryos when compared to the negative control (figure 5G). Remarkably, in some individual embryos, the number of vascular loops observed was even higher than in the bFGF-positive control group. In terms of the SIV bud length, the 52S-BG-treated embryos displayed greater values than the negative control (figure 5H). However, the obtained length was still significantly less than the bFGF-positive stimulated embryos ( $p < 0.007$ ).

### 3.9. PCL/52S-BG composite scaffolds: fabrication and characterization, weight loss, water uptake and ion release

PCL scaffolds containing 10 wt.% 52S-BG were successfully fabricated by additive manufacturing. Macroscopically, PCL and PCL/52S-BG scaffolds had similar morphology and pore shape (figure 6A). The distribution of 52S-BG particles in the PCL matrix was homogenous (figure 6A, glass particles shown in red). All scaffolds featured high porosity with values of  $\geq 76\%$ . However, further investigation revealed that the incorporation of 10 wt.% 52S-BG particles led to increased fiber thickness as well as a minor decrease in total porosity, from  $80.05 \pm 3.7\%$  in PCL scaffolds to  $76.56 \pm 5.98\%$ , and pore size, restricted to 300–700  $\mu\text{m}$  in the PCL/52S-BG scaffolds (figure 6A and B). Interestingly, pores  $> 700 \mu\text{m}$  were present in the plain PCL scaffolds (figure 6B).

Incorporation of 52S-BG particles increased the Young's modulus from 180 MPa in PCL scaffolds to 230 MPa in PCL/52S-BG scaffolds ( $p < 0.0001$ ) when tested in dry conditions (figure 6C). Following incubation in PBS, the Young's modulus of PCL scaffolds displayed a negligible change (up to 28 days of incubation). By contrast, for PCL/52S-BG scaffolds, the Young's modulus significantly decreased at 14 days post-incubation ( $p < 0.05$ ).

The weight loss and water uptake were significantly affected by the incorporation of 52S-BG particles to the scaffolds. Upon PBS incubation, PCL/52S-BG scaffolds displayed an approximately 10% weight loss (figure 6D). In addition, these scaffolds showed a water uptake peak of 200% of the initial scaffold weight at 14 days post-incubation (figure 6E). By contrast, PCL scaffolds displayed negligible weight loss and water uptake after incubation in PBS. In addition, neither scaffold (PCL or PCL/52S-BG) significantly changed the pH of the cell culture media, which slightly fluctuated around pH 8.6 from 3 h up to 7 days of incubation (figure 6F).

Si ions were released gradually from PCL/52S-BG scaffolds, whereas no Si release was detected from the PCL scaffolds (figure 6G). Na increased for both scaffolds during the first 24 h post-incubation, with no differences in Na release when comparing the PCL and PCL/52S-BG scaffolds. P and Ca concentrations were in the same range for both scaffolds and followed similar tendencies to remain unchanged for all the observation times ( $p > 0.05$ ).

### 3.10. Biocompatibility and cytotoxicity of PCL/52S-BG scaffolds to AdMSCs

PCL/52S-BG scaffolds induced significantly less LDH release by AdMSCs compared to the PCL scaffolds (figure 7A,  $p < 0.05$  at 7 days). In agreement with this, the composite scaffolds also displayed a significant increase of attached, metabolically active cells from 3 days of culture onwards (figure 7B). Indeed, at 7 days post-culture, a significantly higher metabolic activity was detected for the cells seeded on the composite scaffolds ( $p < 0.01$ , figure 7B). These results were supported by live/dead staining of 7-day cultures (figure 7C). In addition, seeding efficiency was increased from 11.88% in PCL to 24.41% in PCL/52S-BG scaffolds, indicating that the 52S-BG particles improved cell attachment (figure 7D).

### 3.11. Effect of PLC/52S-BG scaffolds on AdMSC gene and protein expression

Gene expression was evaluated after culture of AdMSCs on PCL and PCL/52S-BG scaffolds. No significant differences were observed between PCL and PCL/52S-BG in terms of the proliferation marker Cyclin D1 or the apoptosis marker Casp3 (figure 7E and F). RunX2 expression appeared to be higher in the PCL/52S-BG scaffolds compared to PCL, although this was not statistically significant (figure 7G). Similar results were observed for ALP expression at 7 days post-culture (figure 7H). No significant difference was observed in osteocalcin expression between the two scaffolds (figure 7I). By contrast, osteopontin, displayed an upregulation in AdMSCs cultured on PCL/52S-BG scaffolds already at 3 days post-culture ( $p < 0.05$ , figure 7J). This early upregulation of osteopontin expression agrees with the results obtained using 52S-BG particles with both, AdMSCs and OBs. Unexpectedly, collagen I expression was downregulated in AdMSCs cultured on PCL/52S-BG scaffolds ( $p < 0.05$  at 14 days, figure 7K). Notably, at days 3 and 7 after AdMSC culture on PCL/52S-BG scaffolds, VEGF gene expression and protein secretion were significantly upregulated compared to PCL scaffolds ( $p < 0.05$ , figure 7L and M).

### 3.12. Mineralized matrix formation by AdMSCs on PCL/52S-BG scaffolds

Abundant mineral deposition was observed on PCL/52S-BG scaffolds at days 21 and 35 after AdMSC culture (figure 8A). By contrast, negligible mineral deposits were observed on PCL scaffolds (figure 8A). At 35 days after *in vitro* culture on PCL/52S-BG scaffolds, the surface of the scaffolds appeared entirely covered by a mineral layer which extended between the pores. SEM observations confirmed the mineral layer deposits on PCL/52S-BG scaffolds (Figure 8B, right panels). In addition, cells could be identified growing inside the cauliflower-like mineral formation. EDX analysis confirmed the

presence of calcium phosphate deposits on the surface of the PCL/52S-BG scaffolds (figure 8C). DOI: 10.1039/D1BM01311D

## 4. Discussion

In this study, a new phosphate-free, silicate-based BG was synthesized and characterized. Synthesis was performed by the conventional melt quenching method. This procedure, although resulting in glasses of less porosity than the ones obtained via sol-gel, is considerably less expensive.<sup>22</sup> In addition, melt quenched glasses exhibit the advantage of superior mechanical properties,<sup>38</sup> a highly desired feature for materials used in bone engineering applications.

The obtained glass material appears to be biocompatible with human primary cells, capable of inducing *in vitro* mineralization and, remarkably, *in vitro* and *in vivo* angiogenesis. A concentration-dependent effect was demonstrated in our study.

BGs are well-known to cause a pH rise when immersed in aqueous solutions.<sup>39</sup> According to Hench,<sup>40</sup> this initial pH spike is an indicator of ion exchange between modifier cations from the BG and protons from the dissolution medium followed by alkaline hydrolysis of Si-O-Si bonds and subsequent formation of silanol (Si-OH) groups. Consequently, the dissolution medium becomes depleted of protons and the pH increases. After just 30 min of immersion in SBF, the pH of the dissolution media increased linearly with increasing 52S-BG particle concentration. However, no significant difference was observed in the Na or Ca concentrations (modifier cations) in all 52S-BG particle groups compared to the control. This is most likely due to the late observation time-point (6 hours after immersion), because the pH spike was observed as early as 30 min after incubation. By contrast, at  $> 200 \mu\text{g/ml}$  52S-BG particles, significantly higher Si was observed compared to the control, indicating that a pH increase to a certain threshold is necessary to disrupt the Si-O-Si glass network.<sup>39</sup> The *in vitro* bioactivity of 52S-BG was confirmed by the presence of calcium phosphate deposits on the glass surface after incubation with SBF.

Cell culture studies showed that 52S-BG particles at a concentration  $< 400 \mu\text{g/ml}$  can support AdMSC and OB growth and proliferation. However, a high 52S-BG concentration (1000  $\mu\text{g/ml}$ ) was cytotoxic to both cell types, most likely because of the rise in the culture media pH and the presence of high concentrations of glass dissolution ionic products. It has been reported that high Si<sup>41</sup> and cytosolic Ca<sup>42</sup> levels can trigger downstream events that induce cell apoptosis. Similar cytotoxicity effects of BGs have been previously reported<sup>43-45</sup> and may be avoided by pre-conditioning the BGs prior to cell culture.<sup>44, 45</sup>

Overall, it was observed that AdMSCs and OBs were differentially regulated by 52S-BG. This may be related to the ions released from the 52S-BG particles. To further elucidate this, the gene expression of cell cycle regulators and osteogenic markers was analyzed. Bcl-2 is a growth-promoting, anti-apoptotic effector while Cyclin D1 promotes cell cycle entry by inducing the G1/S transition. In OBs exposed to 300  $\mu\text{g/ml}$  52S-BG particles, the time-point of highest Bcl-2 expression

coincided with that of Cyclin D1. Xynos *et al.*<sup>46</sup> also observed Cyclin D1 upregulation in OBs after 48 h of culture with 45S5 Bioglass® extracts. In agreement with these findings, Sun *et al.*<sup>47</sup> and Xynos *et al.*<sup>48</sup> demonstrated that the ionic products of 45S5 Bioglass® induced OB proliferation by accelerating the growth cycle through G1/S, resulting in a more rapid G2 entry. Collectively, these results provide new insights into the molecular mechanisms by which BGs affect OB growth and proliferation, which appear to involve Cyclin D1 and Bcl2 but not the cell cycle effector Mcm5, a DNA helicase downstream of Cyclin D1. For AdMSCs, however, it appears that the regulation of cell growth and proliferation may involve other molecules, which need to be further elucidated in future studies.

AdMSCs and OBs displayed the highest osteogenic potential when exposed to 300 µg/ml 52S-BG particles. This indicated that 52S-BG dissolution products were able to induce osteogenesis in these cells. Of note, 52S-BG appeared to act synergistically with β-glycerophosphate and L-ascorbate-2-phosphate to further enhance osteogenesis. This agrees with previous observations by Poh *et al.* who presented two distinctive PCL/BG composite scaffolds with enhanced osteopontin and osteocalcin expression in the presence of β-glycerophosphate and L-ascorbate-2-phosphate supplements.<sup>45</sup>

Although BGs are well-known for their bioactivity and osteogenic potential, wider clinical implementation in orthopedic applications is frequently impeded by their brittleness. Leveraging on the additive manufacturing capability, PCL/52S-BG composite scaffolds were fabricated to harness the bioactivity of 52S-BG while improving the biomaterial bulk mechanical properties. In comparison to PCL scaffolds, PCL/52S-BG composite scaffolds featured thicker microfilaments and smaller pore size, resulting in an approximately 5% decrease in total porosity. During the scaffold fabrication process, the extrusion temperature for the composite was slightly higher than for PCL, causing a delayed solidification and resulting in microfilament sagging and increased filament size.<sup>19</sup> Although there were small changes in the scaffold morphology, the porosity and pore size remained within the optimal range for bone tissue engineering applications (100–500 µm pores<sup>1</sup> and 50–90% porosity<sup>49</sup>). The homogenous incorporation of 10 wt.% 52S-BG particles into the PCL bulk improved the compressive Young's modulus of PCL/52S-BG scaffolds compared to PCL scaffolds. The increased microfilament thickness and reduced porosity in PCL/52S-BG scaffolds could also contribute to the enhanced PCL/52S-BG scaffolds' compressive Young's modulus. These results are in agreement with the those obtained by Poh *et al.*,<sup>19,26</sup> Korpela *et al.*<sup>50</sup> and Jiang *et al.*,<sup>51</sup> who incorporated various types of BGs or hydroxyapatite particles into PCL. After 14 or 28 days in PBS, the compressive Young's modulus of the PCL/52S-BG scaffolds decreased most probably because of the dissolution of 52S-BG particles coupled with insufficient glass-polymer interaction. Modifying the PCL or BG to increase their interfacial bonding may help to improve the scaffolds' mechanical properties under physiological conditions.<sup>52</sup> Although the Young's modulus of the fabricated PCL/52S-BG scaffolds remains significantly lower

than that of native bone tissue (0.05–0.5 GPa in trabecular bone and 7–30 GPa in cortical bone<sup>1</sup>), we have shown that increased stiffness compared to PCL scaffolds improved mechanical resistance and could promote osteogenic differentiation *in vitro*, consistent with the findings of other studies.<sup>53,54</sup>

We found that AdMSC attachment, proliferation, osteogenic differentiation and mineralized matrix formation were significantly enhanced in PCL/52S-BG composite scaffolds compared to PCL scaffolds. This may be attributed to several factors. Water uptake into PCL/52S-BG scaffolds significantly increased after 7 days of incubation in PBS compared to PCL scaffolds, indicating improved hydrophilicity and thereby better support of cell attachment.<sup>55,56</sup> Secondly, the dissolution ionic products from 52S-BG particles embedded within the PCL bulk may have contributed towards the improved osteogenic differentiation of AdMSCs. The occurrence of physical-chemical reactions (e.g. crystallization of Ca-P on scaffold surfaces) enables the interaction of collagen molecules with the scaffold surface and triggers cascades of events favoring AdMSC adhesion, proliferation, differentiation and matrix deposition.<sup>57</sup> In addition, 52S-BG incorporation may lead to an increase in surface roughness, which is favorable for cell attachment and proliferation.<sup>43,58</sup>

Not surprisingly, osteogenic RunX2 and osteopontin expression appeared to be better supported by the PCL/52S-BG composite scaffold than by the 52S-BG particles alone. This may be related to the 3D structure and topography of the scaffolds. It has been reported that scaffold topography and stiffness can significantly affect gene expression.<sup>59</sup> Another important difference was regarding the ion release. Overall, ions were released from the composite scaffolds over a long time period. Si, for example, was released slower and more progressively from PCL/52S-BG scaffolds when compared to the glass particles suspension. In this regard, is well-documented that ionic dissolution products of BGs, such as Si and Ca, are capable of inducing osteogenesis *in vitro* (reviewed in<sup>3</sup>).

The success rate of bone regeneration and remodeling is highly dependent on the extent of vascularization, particularly for critical-sized bone defects.<sup>60</sup> Therefore, angiogenesis is a much-desired feature in bone substitute materials. We found that 52S-BG particles upregulated VEGF expression in AdMSCs and OBs as early as 3 days after culture. Interestingly, a second but lower bout was observed. We did not find similar evidence in current bioactive glass literature. We speculate that this second VEGF upregulation might be due to the agglomeration formed between the cells and the BG particles at later times after culture. The originated cell-particle mass may have created relative hypoxia responsible for this second VEGF increase observed at 14 days post-stimulation.

Strikingly, these particles were also able to induce vessel formation *in vivo* in a zebrafish embryo to a similar extent as bFGF. This evidence supports a robust angiogenic potential of these new glass particles, which was retained after the composite scaffold fabrication. PCL/52S-BG composite scaffolds promoted VEGF protein release by AdMSCs. This angiogenic characteristic may also be associated with ion release from the 52S-BG particles. It was proposed by Zhai *et al.*<sup>61</sup> that Si plays a

major role in the induction of blood vessel formation. In an elegantly presented review article, Kargozar *et al.* described the angiogenic potential of silicate-based BGs.<sup>11</sup> Our glass, being rich in Si (52 wt.%), may thus be provided with superior angiogenic properties. Overall, the data presented here suggest that neither P<sub>2</sub>O<sub>5</sub> groups nor metallic dopants may be needed in 52S-BG to be angiogenic while retaining its osteogenic features. Further investigations should focus on in-depth ion release and degradation, in particular given that this material contains trace elements that conferred minimal crystallinity. *In vivo* testing using a relevant bone defect model should also be considered to confirm osteogenic and angiogenic properties.

## Conclusions

The BG presented in this paper, that is 52S-BG may be of interest for clinical application based on its combined osteogenic and angiogenic properties. Furthermore, the possibility of combining 52S-BG with polymers to obtain a 3D composite scaffold may be highly relevant for the repair of large bone segmental defects. *In vivo* studies in, for example, small animal fracture models may be relevant to unravel the translational potential of this novel material.

## Author Contributions

Conceptualization: E.R.B. Formal analysis: S.F.T., P.S.P.P., M.v.G., E.R.B. Funding acquisition: A.G., M.v.G., E.R.B. Investigation: S.F.T., J.A.D., P.S.P.P., W.Z., M.G.-V., L.M. Project administration: M.v.G., E.R.B. Resources: S.M., A.G., M.v.G. Supervision: E.R.B. Visualization: S.F.T., E.R.B. Writing (original draft): S.F.T., E.R.B. Writing (review & editing): all authors.

## Conflicts of interest

There are no conflicts to declare.

## Acknowledgements

This study was partially funded by the Zeidler foundation (Grant ID: Regentesis). The authors acknowledge the support received from BAYLAT – CONICET for the collaborative work between the universities in Bavaria, Germany and Salta, Argentina.

## References

1. L.-C. Gerhardt and A. R. Boccaccini, *Materials*, 2010, **3**, 3867.
2. L. L. Hench, R. J. Splinter, W. C. Allen and T. K. Greenlee, *J Biomed Mater Res*, 1971, **5**, 117-141.
3. A. Hoppe, N. S. Guldal and A. R. Boccaccini, *Biomaterials*, 2011, **32**, 2757-2774.
4. X. Zhou, N. Zhang, S. Mankoci and N. Sahai, *J Biomed Mater Res A*, 2017, **105**, 2090-2102.
5. M. Julien, S. Khoshniat, A. Lacreusette, M. Gatius, A. Bozec, E. F. Wagner, Y. Wittrant, M. Masson, P. Weiss, J. Beck, D. Magne and J. Guicheux, *J Bone Miner Res*, 2009, **24**, 1856-1868.
6. B. Cabal, L. Alou, F. Cafini, R. Couceiro, D. Sevilano, L. Esteban-Tejeda, F. Guitian, R. Torrecillas and J. S. Moya, *Sci Rep*, 2014, **4**, 5440.
7. J. R. Jones, O. Tsigkou, E. E. Coates, M. M. Stevens, J. M. Polak and L. L. Hench, *Biomaterials*, 2007, **28**, 1653-1663.
8. M. Suarez, E. Fernandez-Garcia, A. Fernandez, R. Lopez-Piriz, R. Diaz and R. Torrecillas, *Sci Rep*, 2020, **10**, 13171.
9. J. R. Jones and L. L. Hench, *J Biomed Mater Res B Appl Biomater*, 2004, **68**, 36-44.
10. D. Lukito, J. M. Xue and J. Wang, *Mater Lett*, 2005, **59**, 3267-3271.
11. S. Kargozar, F. Baino, S. Hamzehlou, R. G. Hill and M. Mozafari, *Trends Biotechnol*, 2018, **36**, 430-444.
12. G. Bühner, U. Rottensteiner, A. Hoppe, R. Detsch, D. Dafinova, T. Fey, P. Greil, C. Weis, J. P. Beier, A. R. Boccaccini, R. E. Horch and A. Arkudas, *Biomed Glas*, 2016, **2**.
13. S. Kargozar, N. Lotfibakhshaiesh, J. Ai, M. Mozafari, P. Brouki Milan, S. Hamzehlou, M. Barati, F. Baino, R. G. Hill and M. T. Joghataei, *Acta Biomater*, 2017, **58**, 502-514.
14. L. A. Haro Durand, G. E. Vargas, N. M. Romero, R. Vera-Mesones, J. M. Porto-Lopez, A. R. Boccaccini, M. P. Zago, A. Baldi and A. Gorustovich, *J Mater Chem B*, 2015, **3**, 1142-1148.
15. A. Hoppe, A. Brandl, O. Bleiziffer, A. Arkudas, R. E. Horch, B. Jokic, D. Janackovic and A. R. Boccaccini, *Mater Sci Eng C Mater Biol Appl*, 2015, **57**, 157-163.
16. E. Littmann, H. Autefage, A. K. Solanki, C. Kallepitis, J. R. Jones, M. Alini, M. Peroglio and M. M. Stevens, *J Eur Ceram Soc*, 2018, **38**, 877-886.
17. M. N. Rahaman, W. Xiao and W. Huang, *Biomed Glas*, 2017, **3**, 56-66.
18. L. L. Hench and J. R. Jones, *Front Bioeng Biotechnol*, 2015, **3**, 194.
19. P. S. Poh, D. W. Hutmacher, M. M. Stevens and M. A. Woodruff, *Biofabrication*, 2013, **5**, 045005.
20. E. R. Balmayor, I. Pashkuleva, A. M. Frias, H. S. Azevedo and R. L. Reis, *J R Soc Interface*, 2011, **8**, 896-908.
21. D. Mondal, M. Griffith and S. S. Venkatraman, *Int J Polym Mater*, 2016, **65**, 255-265.
22. L. Morejón, J. A. Delgado, M. García-Vallés, S. Martínez Manent, E. R. Balmayor and M. van Griensven, *Int J Mater Res*, 2019, **110**, 333-342.
23. T. Kokubo, H. Kushitani, S. Sakka, T. Kitsugi and T. Yamamuro, *J Biomed Mater Res*, 1990, **24**, 721-734.
24. A. Liu, Z. Hong, X. Zhuang, X. Chen, Y. Cui, Y. Liu and X. Jing, *Acta Biomater*, 2008, **4**, 1005-1015.
25. S. K. Misra, D. Mohn, T. J. Brunner, W. J. Stark, S. E. Philip, I. Roy, V. Salih, J. C. Knowles and A. R. Boccaccini, *Biomaterials*, 2008, **29**, 1750-1761.
26. P. S. P. Poh, D. W. Hutmacher, B. M. Holzappel, A. K. Solanki, M. M. Stevens and M. A. Woodruff, *Acta Biomater*, 2016, **30**, 319-333.
27. G. A. Silva, F. J. Costa, N. M. Neves, O. P. Coutinho, A. C. Dias and R. L. Reis, *J Biomed Mater Res A*, 2005, **73**, 234-243.
28. S. Schneider, M. Unger, M. van Griensven and E. R. Balmayor, *Eur J Med Res*, 2017, **22**, 17.

29. S. Payr, E. Rosado-Balmayor, T. Tiefenboeck, T. Schuseil, M. Unger, C. Seeliger and M. van Griensven, *J Orthop Surg Res*, 2021, **16**, 13.
30. R. R. Pochampally, J. R. Smith, J. Ylostalo and D. J. Prockop, *Blood*, 2004, **103**, 1647-1652.
31. A. Oskowitz, H. McFerrin, M. Gutschow, M. L. Carter and R. Pochampally, *Stem Cell Res*, 2011, **6**, 215-225.
32. B. Y. Binder, J. E. Sagun and J. K. Leach, *Stem Cell Rev Rep*, 2015, **11**, 387-393.
33. F. Langenbach and J. Handschel, *Stem Cell Res Ther*, 2013, **4**, 117.
34. E. R. Balmayor, T. E. Baran, M. Unger, A. P. Marques, H. S. Azevedo and R. L. Reis, *J Biomed Mater Res B Appl Biomater*, 2015, **103**, 1610-1620.
35. F. K. Chan, K. Moriwaki and M. J. De Rosa, *Methods Mol Biol*, 2013, **979**, 65-70.
36. M. Kamei, S. Isogai, W. Pan and B. M. Weinstein, *Methods Cell Biol*, 2010, **100**, 27-54.
37. E. A. De Maeyer and R. M. Verbeeck, *J Biomed Mater Res*, 2001, **57**, 467-472.
38. G. Kaur, G. Pickrell, N. Sriranganathan, V. Kumar and D. Homa, *J Biomed Mater Res B Appl Biomater*, 2016, **104**, 1248-1275.
39. D. S. Brauer, *Angew Chem Int Ed Engl*, 2015, **54**, 4160-4181.
40. L. L. Hench, *J Am Ceram Soc*, 1991, **74**, 1487-1510.
41. S. I. Anderson, PhD, Nottingham, 2001, <http://eprints.nottingham.ac.uk/13541/>.
42. C. S. Adams, K. Mansfield, R. L. Perlot and I. M. Shapiro, *J Biol Chem*, 2001, **276**, 20316-20322.
43. J. Rodenas-Rochina, J. L. Ribelles and M. Lebourg, *J Mater Sci Mater Med*, 2013, **24**, 1293-1308.
44. S. Midha, T. B. Kim, W. van den Bergh, P. D. Lee, J. R. Jones and C. A. Mitchell, *Acta Biomater*, 2013, **9**, 9169-9182.
45. P. S. Poh, D. W. Hutmacher, B. M. Holzapfel, A. K. Solanki, M. M. Stevens and M. A. Woodruff, *Acta Biomater*, 2016, **30**, 319-333.
46. I. D. Xynos, A. J. Edgar, L. D. Bותרy, L. L. Hench and J. M. Polak, *J Biomed Mater Res*, 2001, **55**, 151-157. View Article Online  
DOI: 10.1002/jbm.b.10131
47. J. Y. Sun, Y. S. Yang, J. Zhong and D. C. Greenspan, *J Tissue Eng Regen Med*, 2007, **1**, 281-286.
48. I. D. Xynos, A. J. Edgar, L. D. Bותרy, L. L. Hench and J. M. Polak, *Biochem Biophys Res Commun*, 2000, **276**, 461-465.
49. J. Y. Kim and D.-W. Cho, *Microsyst. Technol.*, 2009, **15**, 843-851.
50. J. Korpela, A. Kokkari, H. Korhonen, M. Malin, T. Narhi and J. Seppala, *J Biomed Mater Res B Appl Biomater*, 2013, **101**, 610-619.
51. W. Jiang, J. Shi, W. Li and K. Sun, *J Biomater Sci Polym Ed*, 2013, **24**, 539-550.
52. A. J. Harmata, C. L. Ward, K. J. Zienkiewicz, J. C. Wenke and S. A. Guelcher, *J Mater Res*, 2014, **29**, 2398-2407.
53. C. Yang, M. W. Tibbitt, L. Basta and K. S. Anseth, *Nat Mater*, 2014, **13**, 645-652.
54. A. J. Engler, S. Sen, H. L. Sweeney and D. E. Discher, *Cell*, 2006, **126**, 677-689.
55. M. Hafezi, S. Safarian, M. T. Khorasani and N. A. Abu Osman, *RSC Adv*, 2016, **6**, 35815-35824.
56. B. Lei, K. H. Shin, D. Y. Noh, Y. H. Koh, W. Y. Choi and H. E. Kim, *J Biomed Mater Res B Appl Biomater*, 2012, **100**, 967-975.
57. A. E. Clark, L. L. Hench and H. A. Paschall, *J Biomed Mater Res*, 1976, **10**, 161-174.
58. W. Yang, W. Han, W. He, J. Li, J. Wang, H. Feng and Y. Qian, *Mater Sci Eng C Mater Biol Appl*, 2016, **60**, 45-53.
59. R. A. Perez and G. Mestres, *Mater Sci Eng C Mater Biol Appl*, 2016, **61**, 922-939.
60. J. Henkel, M. A. Woodruff, D. R. Epari, R. Steck, V. Glatt, I. C. Dickinson, P. F. Choong, M. A. Schuetz and D. W. Hutmacher, *Bone Res*, 2013, **1**, 216-248.
61. W. Zhai, H. Lu, L. Chen, X. Lin, Y. Huang, K. Dai, K. Naoki, G. Chen and J. Chang, *Acta Biomater*, 2012, **8**, 341-349.

## ARTICLE

## Tables

**Table 1.** Experimental setup: *in vitro* cell culture and *in vivo* angiogenesis

<i>52S-BG particles</i>					
Assay	Cell type		Zebrafish embryo	Type of culture media	52S-BG concentration (µg/ml)
	AdMSCs	OBs			
Live/dead staining	√	√	-	expansion	
Cytotoxicity (MTT)	√	√	-	expansion	100, 200, 300, 400, 1000
Cell proliferation (PicoGreen)	√	√	-	expansion	
ALP activity	√	√	-	serum starvation (± βGlyP and AA)	100, 200, 300, 400
Matrix mineralization (Alizarin RedS)	√	-	-	serum starvation (± βGlyP and AA)	100 and 300
Gene expression (qPCR)	√	√	-	serum starvation (± βGlyP and AA)	100 and 300
VEGF protein (ELISA)	√	-	-	serum starvation (+ βGlyP and AA)	300
Angiogenesis (functional assay)	-	-	√	Embryonic medium	100
<i>PCL and PCL/52S-BG scaffolds</i>					
Assay	Cell type: AdMSCs		Type of culture media		
Live/dead staining	√		expansion		
Cytotoxicity (MTT and LDH)	√		expansion		
Matrix mineralization (von Kossa)	√		serum starvation (+ βGlyP and AA)		
Gene expression (qPCR)	√		serum starvation (+ βGlyP and AA)		
VEGF protein (ELISA)	√		serum starvation (+ βGlyP and AA)		

**Abbreviations:** βGlyP = β-Glycerophosphate, AA = L-Ascorbate-2-phosphate, human AdMSCs = Human adipose-derived mesenchymal stromal cells, human OBs = Human osteoblasts, MTT = 3-(4,5-dimethylthiazol-2-yl)-2,5-diphenyltetrazolium bromide, ALP = Alkaline phosphatase, qPCR = Real-time quantitative polymerase chain reaction, VEGF = Vascular endothelial growth factor, ELISA = Enzyme-linked immunosorbent assay, LDH = Lactate dehydrogenase, PCL = Poly-ε-caprolactone.

**Table 2.** Composition of obtained 52S-BG as determined by X-ray fluorescence, mean  $\pm$  standard deviation (SD). Of note, the 52S-BG was obtained using natural origin precursors, that is silica sand and calcite minerals. This fact may explain the presence of diverse trace elements found in the glass

Oxide	SiO <sub>2</sub>	Na <sub>2</sub> O	CaO	Al <sub>2</sub> O <sub>3</sub>	MgO	TiO <sub>2</sub>	Fe <sub>2</sub> O <sub>3</sub>	P <sub>2</sub> O <sub>5</sub>	K <sub>2</sub> O
wt.% $\pm$	52.1 $\pm$	23.2 $\pm$	22.6 $\pm$	0.26 $\pm$	0.16 $\pm$	0.06 $\pm$	0.032 $\pm$	0.024 $\pm$	0.011 $\pm$
SD	0.3	0.1	0.5	0.04	0.01	0.005	0.003	0.003	0.002

### Figure legends

**Figure 1. Characterization of 52S-BG particles, *in vitro* bioactivity and ion release.** **A)** Representative XRD spectrum of the 52S-BG discs, **B)** TG-DTA curve showing 52S-BG weight and energy release with increasing temperature, **C)** *in vitro* bioactivity analysis of 52S-BG discs by SEM (left) and EDX (right) showing mineral deposition on the glass surface after 15 days of incubation in SBF and **D)** pH of DMEM medium on incubation with 0–1000  $\mu$ g/ml 52S-BG particles ( $n = 6$ , mean  $\pm$  SEM). **E)** Cumulative release of Si, Na, Ca and P ions from 52S-BG particles (0–1000  $\mu$ g/ml). The ion release was investigated in DMEM medium without further supplementation. The data were normalized to the DMEM ionic concentration ( $n = 3$ , mean  $\pm$  SEM).

**Figure 2. *In vitro* biocompatibility of 52S-BG particles evaluated on human adipose-derived mesenchymal stem cells (AdMSCs) and osteoblasts (OBs).** Metabolic activity of **A)** AdMSCs and **B)** OBs after 1, 3 or 7 days of culture in the presence of 100–1000  $\mu$ g/ml 52S-BG particles. Dashed line indicates 100% viable cells (i.e. cells cultured in medium without glass particles). Results are reported as mean  $\pm$  SEM. **C)** Calcein AM/PI/Hoechst staining of AdMSCs and OBs after 7 days of culture with 52S-BG particles (100–1000  $\mu$ g/ml) showing viable cells (green), apoptotic cells (red) and cell nuclei (blue). Cell proliferation of **D)** AdMSCs and **E)** OBs cultured in the presence of 100–400  $\mu$ g/ml 52S-BG particles. Results are expressed as ng/ $\mu$ l of dsDNA and reported as the mean  $\pm$  SEM. \*  $p < 0.05$ , \*\*\*  $p < 0.001$ , \*\*\*\*  $p < 0.0001$ .

**Figure 3. ALP activity and mineralization of human adipose-derived mesenchymal stem cells (AdMSCs) and human osteoblasts (OBs) after exposure to various 52S-BG particle concentrations.** ALP activity in **A), B)** AdMSCs and **C), D)** OBs cultured with 100, 200, 300 or 400  $\mu$ g/ml 52S-BG particles. The effect of adding  $\beta$ -glycerophosphate ( $\beta$ GlyP) and L-ascorbate-2-phosphate (AA) is shown. ALP results are expressed as fold change to control samples (mean  $\pm$  SEM). Cell cultures without 52S-BG particles were used as a control (dashed line). **E)** Alizarin Red S staining of AdMSCs cultured for 14, 21 or 35 days in presence of 100 or 300  $\mu$ g/ml 52S-BG particles. 52S-BG particles incubated in cell culture medium was used as a material control. Scale bars = 600  $\mu$ m. **F)** Alizarin Red S quantification reported as mg/ml of hexadecylpyridiniumchloride (mean  $\pm$  SEM). Statistical significance is indicated by \*  $p < 0.05$ . **G)** SEM image (left) and EDX semi-quantification of mineral deposits (right) observed on the AdMSC extracellular matrix when exposed to 300  $\mu$ g/ml 52S-BG particles.

**Figure 4. Gene expression analysis of proliferation, apoptosis and osteogenesis in human adipose-derived mesenchymal stem cells (AdMSCs) and human osteoblasts (OBs) exposed to 100 or 300  $\mu$ g/ml 52S-BG particles.** **A), B)** Proliferation- and apoptosis-related markers, Cyclin D1 and Casp3, respectively. **C) – H)** Osteogenesis-related markers, RunX2, ALP, osteocalcin, osteopontin and collagen I. The effect of adding  $\beta$ -glycerophosphate ( $\beta$ GlyP) and L-ascorbate-2-phosphate (AA) is shown. Gene expression is expressed as fold change (mean  $\pm$  SEM) of ddC<sub>t</sub> values ( $2^{-ddCt}$ ) with respect to the control sample (dashed line). \*  $p < 0.05$ , \*\*  $p < 0.01$ , \*\*\*\*  $p < 0.0001$ .

**Figure 5. *In vitro* and *in vivo* angiogenic properties of the 52S-BG particles.** **A)** VEGF gene expression in human adipose-derived mesenchymal stem cells (AdMSCs) and human osteoblasts (OBs) after culture in the presence of 100 or 300  $\mu$ g/ml 52S-BG particles for 3, 7 or 14 days. The effect of adding  $\beta$ -glycerophosphate ( $\beta$ GlyP) and L-ascorbate-2-phosphate (AA) is shown. Results are expressed as fold change (mean  $\pm$  SEM) of ddC<sub>t</sub> values ( $2^{-ddCt}$ ) with respect to the control sample (dashed line). \*\*\*  $p < 0.001$ . **B)** VEGF production by AdMSCs at 3, 7 and 14 days after stimulation with 300  $\mu$ g/ml 52S-BG particles. Results are expressed as pg VEGF normalized to the total protein content (mean  $\pm$  SEM). \*\*  $p < 0.01$ . **C) – E)** Subintestinal vascular plexus of zebrafish embryos 72 hpf (side view) at 24 h post-stimulation with the ionic dissolution products from the 52S-BG particles. The sub-intestinal vein (SIV) used for semi-quantification purposes is shown within the dashed squares. Representative images are shown for negative control, 52S-BG particles and positive bFGF control. Scale bars = 500  $\mu$ m. Results of the Fiji quantification are presented as a boxplot with whiskers from minimum to maximum: **F)** SIV area, **G)** number of compartments per SIV and **H)** length of the SIV basket. \*  $p < 0.05$  and \*\*\*  $p < 0.001$ .  $n = 60$  individual zebrafish embryos were analyzed per group.

**Figure 6. Characterization of PCL/52S-BG composite scaffolds.** **A)** 3D  $\mu$ CT reconstruction image showing the microstructure of the obtained PCL (left side; side and frontal views) and PCL/52S-BG (right side) scaffolds. Red dots, indicating embedded 52S-BG particles, illustrate the distribution of the glass within the PCL matrix (white). Total and open porosity percentage are reported in a table below the images. **B)** Filament thickness and pore size of the obtained PCL and PCL/52S-BG scaffolds as calculated by  $\mu$ CT ( $n = 6$ ; mean  $\pm$  SEM). **C)** Mechanical characterization of PCL and PCL/52S-BG scaffolds shown by the Young's modulus (mean  $\pm$  SEM, MPa). Scaffolds were tested before ( $t = 0$  days) and after ( $t = 14$  or 28 days) of immersion in PBS. Also depicted are the stress-strain curves obtained

for PCL and PCL/52S-BG scaffolds before ( $t = 0$  days) immersion in PBS.  $n = 8$  scaffolds per group were used for the mechanical analysis. **D)** Weight loss and **E)** water uptake of PCL and PCL/52S-BG scaffolds upon 28 days of incubation in PBS. Results are expressed as the percentage of either weight loss or weight gain ( $n = 8$ ; mean  $\pm$  SEM). **F)** pH variation of low glucose DMEM as a result of incubation of PCL or PCL/52S-BG scaffolds for up to 7 days ( $n = 3$ ; mean  $\pm$  SEM). **G)** Cumulative release of Si, Na, Ca and P ions from PCL and PCL/52S-BG scaffolds upon incubation in low glucose DMEM for up to 7 days. The data were normalized to the DMEM ionic concentration ( $n = 3$ ; mean  $\pm$  SEM). \*  $p < 0.05$ , \*\*  $p < 0.01$ , \*\*\*  $p < 0.001$ , \*\*\*\*  $p < 0.0001$ .

**Figure 7. Biocompatibility and gene expression of AdMSCs cultured on PCL/52S-BG composite scaffolds.** **A)** LDH release, **B)** metabolic activity (MTT test) and **C)** calcein AM/PI staining analysis performed for AdMSCs cultured on PCL or PCL/52S-BG scaffolds for up to 7 days. Fluorescence microscopy images show viable cells in green and apoptotic cells in red. **D)** Seeding efficiency of AdMSCs on PCL and PCL/52S-BG scaffolds. The results are expressed as the percentage of cells attached to the scaffold surface at 24 h after seeding with respect to the total cell population. **E) – L)** Gene expression of the proliferation and apoptosis markers Cyclin D1 and Casp3, respectively, as well as the osteogenic markers RunX2, ALP, osteocalcin, osteopontin and collagen I and the angiogenic marker VEGF. Gene expression is reported as fold change of  $dC_t$  values ( $2^{-dC_t}$ ) with respect to the housekeeping gene  $\beta$ -tubulin. **M)** VEGF production by AdMSCs cultured on PCL or PCL/52S-BG composite scaffolds. VEGF protein quantification in the cell supernatant was normalized to the total protein content (mean  $\pm$  SEM). \*  $p < 0.05$ , \*\*\*  $p < 0.001$ ,  $n = 3$  scaffolds used for analysis.

**Figure 8. Mineralization of AdMSCs cultured on PCL/52S-BG composite scaffolds.** **A)** von Kossa staining of AdMSCs cultured on PCL and PCL/52S-BG scaffolds for 21 or 35 days. Matrix deposits can be identified occluding the pores of the PCL/52S-BG composite scaffolds. **B)** SEM images of the AdMSC-seeded scaffolds after 35 days of *in vitro* culture. Higher magnification images at the bottom of the figure show cells adhered to the scaffold surface as well as cellular matrix deposition. **C)** EDX semi-quantification of mineral deposits found on the surface of PCL/52S-BG scaffolds.



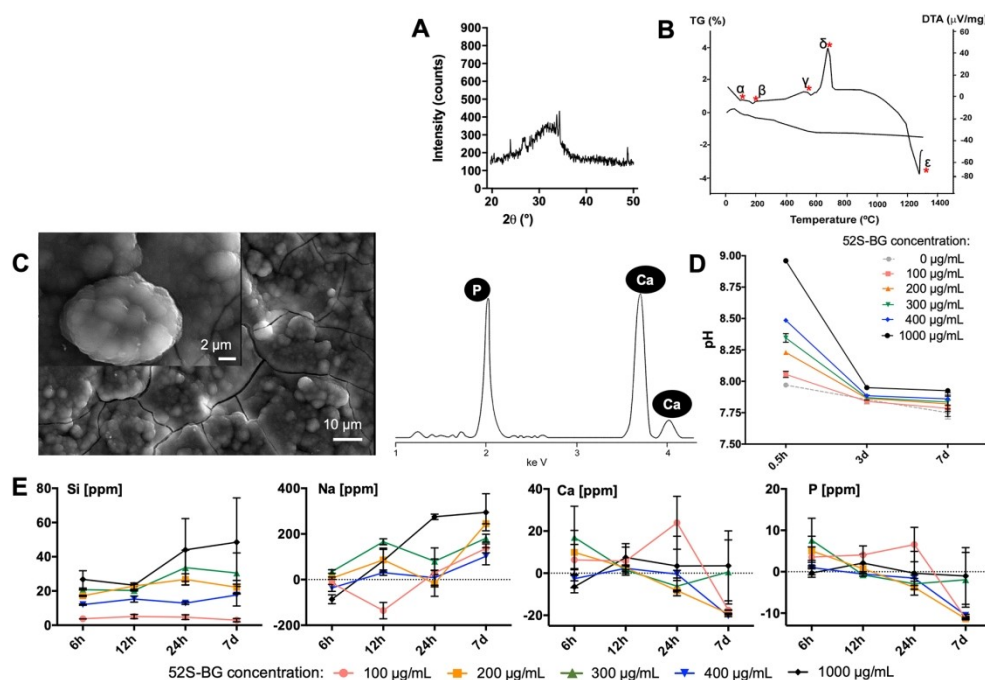


Figure 1. Characterization of 52S-BG particles, in vitro bioactivity and ion release. A) Representative XRD spectrum of the 52S-BG discs, B) TG-DTA curve showing 52S-BG weight and energy release with increasing temperature, C) in vitro bioactivity analysis of 52S-BG discs by SEM (left) and EDX (right) showing mineral deposition on the glass surface after 15 days of incubation in SBF and D) pH of DMEM medium on incubation with 0–1000  $\mu\text{g}/\text{mL}$  52S-BG particles ( $n = 6$ , mean  $\pm$  SEM). E) Cumulative release of Si, Na, Ca and P ions from 52S-BG particles (0–1000  $\mu\text{g}/\text{mL}$ ). The ion release was investigated in DMEM medium without further supplementation. The data were normalized to the DMEM ionic concentration ( $n = 3$ , mean  $\pm$  SEM).

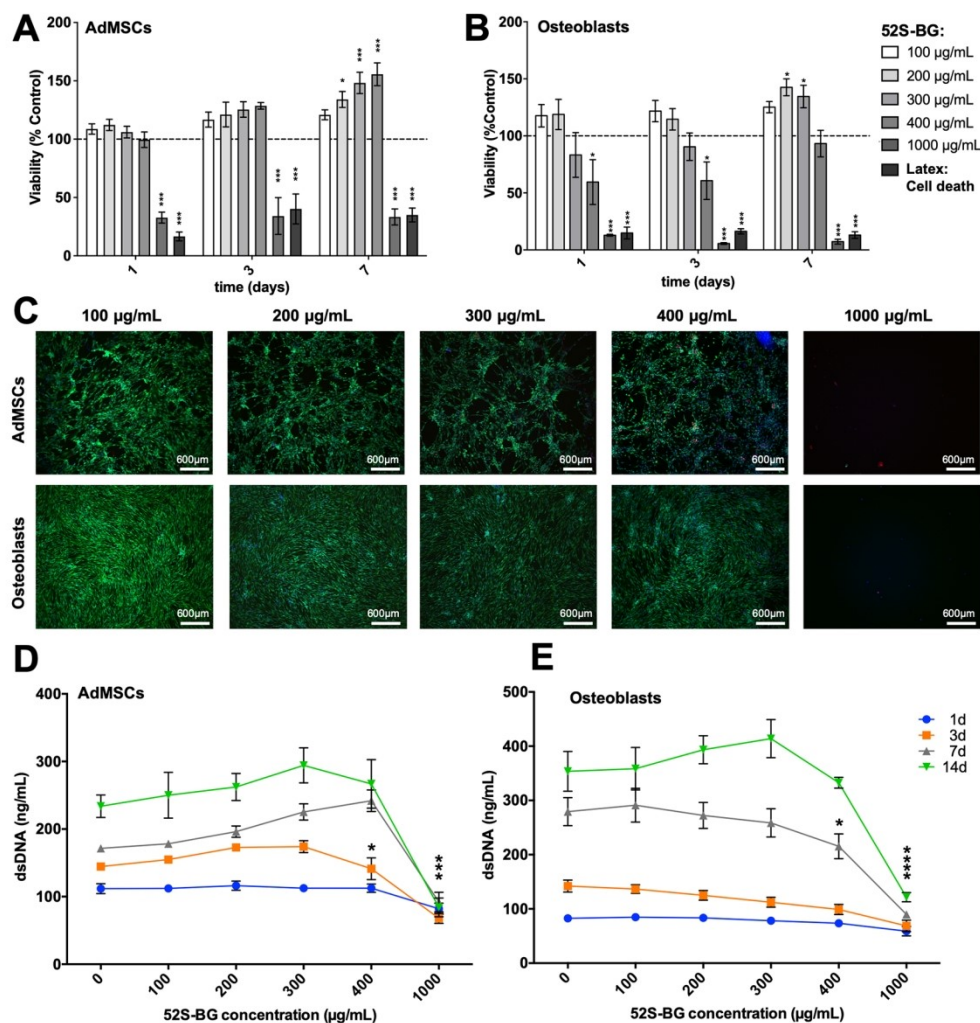


Figure 2. In vitro biocompatibility of 52S-BG particles evaluated on human adipose-derived mesenchymal stem cells (AdMSCs) and osteoblasts (OBs). Metabolic activity of A) AdMSCs and B) OBs after 1, 3 or 7 days of culture in the presence of 100–1000 µg/ml 52S-BG particles. Dashed line indicates 100% viable cells (i.e. cells cultured in medium without glass particles). Results are reported as mean  $\pm$  SEM. C) Calcein AM/PI/Hoechst staining of AdMSCs and OBs after 7 days of culture with 52S-BG particles (100–1000 µg/ml) showing viable cells (green), apoptotic cells (red) and cell nuclei (blue). Cell proliferation of D) AdMSCs and E) OBs cultured in the presence of 100–400 µg/ml 52S-BG particles. Results are expressed as ng/ $\mu$ l of dsDNA and reported as the mean  $\pm$  SEM. \*  $p < 0.05$ , \*\*\*  $p < 0.001$ , \*\*\*\*  $p < 0.0001$ .

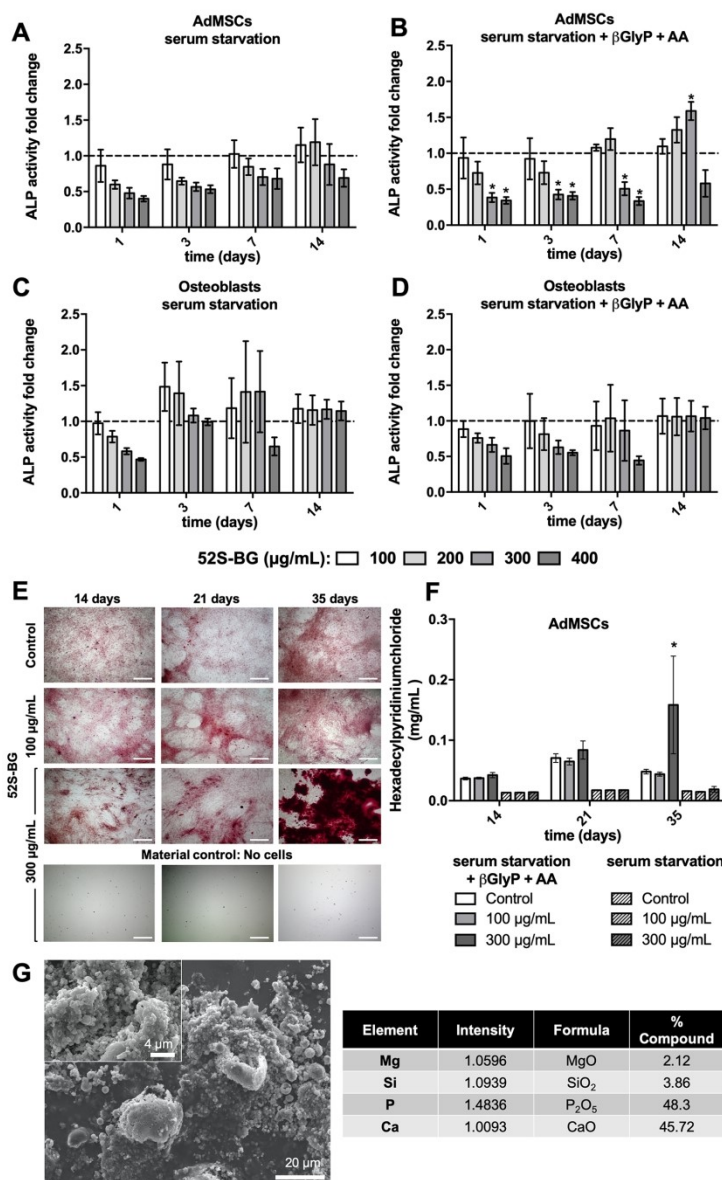


Figure 3. ALP activity and mineralization of human adipose-derived mesenchymal stem cells (AdMSCs) and human osteoblasts (OBs) after exposure to various 52S-BG particle concentrations. ALP activity in A), B) AdMSCs and C), D) OBs cultured with 100, 200, 300 or 400  $\mu$ g/ml 52S-BG particles. The effect of adding  $\beta$ -glycerophosphate ( $\beta$ GlyP) and L-ascorbate-2-phosphate (AA) is shown. ALP results are expressed as fold change to control samples (mean  $\pm$  SEM). Cell cultures without 52S-BG particles were used as a control (dashed line). E) Alizarin Red S staining of AdMSCs cultured for 14, 21 or 35 days in presence of 100 or 300  $\mu$ g/ml 52S-BG particles. 52S-BG particles incubated in cell culture medium was used as a material control. Scale bars = 600  $\mu$ m. F) Alizarin Red S quantification reported as mg/ml of hexadecylpyridiniumchloride (mean  $\pm$  SEM). Statistical significance is indicated by \*  $p < 0.05$ . G) SEM image (left) and EDX semi-quantification of mineral deposits (right) observed on the AdMSC extracellular matrix when exposed to 300  $\mu$ g/ml 52S-BG particles.

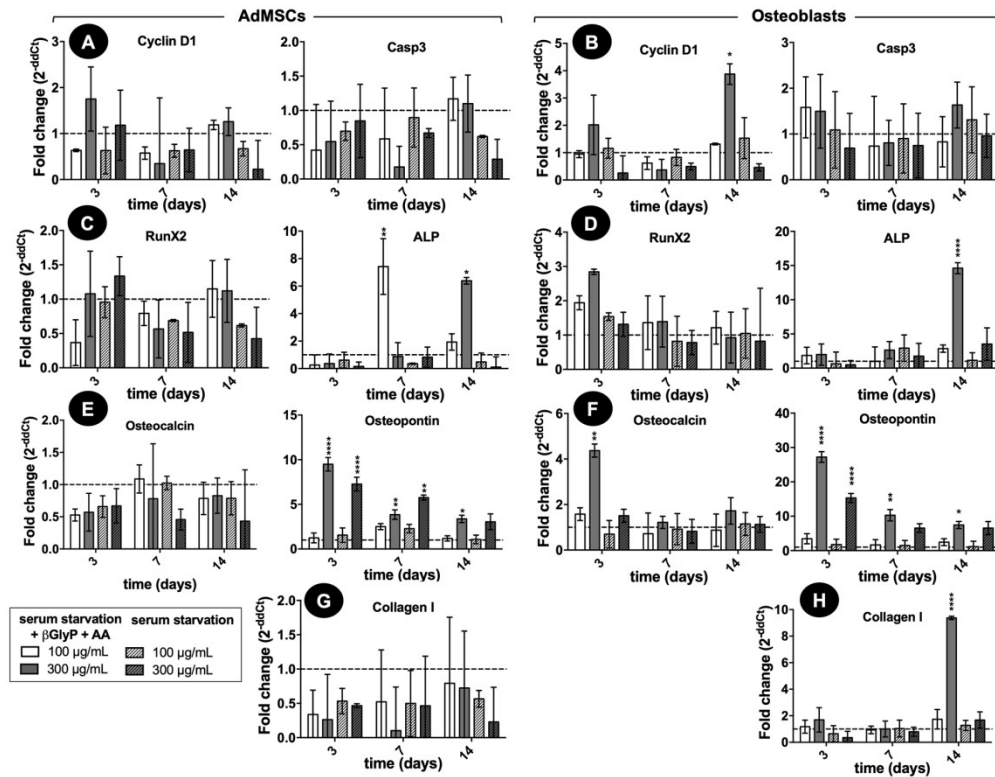


Figure 4. Gene expression analysis of proliferation, apoptosis and osteogenesis in human adipose-derived mesenchymal stem cells (AdMSCs) and human osteoblasts (OBs) exposed to 100 or 300  $\mu$ g/ml 52S-BG particles. A), B) Proliferation- and apoptosis-related markers, Cyclin D1 and Casp3, respectively. C) – H) Osteogenesis-related markers, RunX2, ALP, osteocalcin, osteopontin and collagen I. The effect of adding  $\beta$ -glycerophosphate ( $\beta$ GlyP) and L-ascorbate-2-phosphate (AA) is shown. Gene expression is expressed as fold change (mean  $\pm$  SEM) of ddCt values ( $2^{-ddCt}$ ) with respect to the control sample (dashed line). \*  $p < 0.05$ , \*\*  $p < 0.01$ , \*\*\*  $p < 0.0001$ .

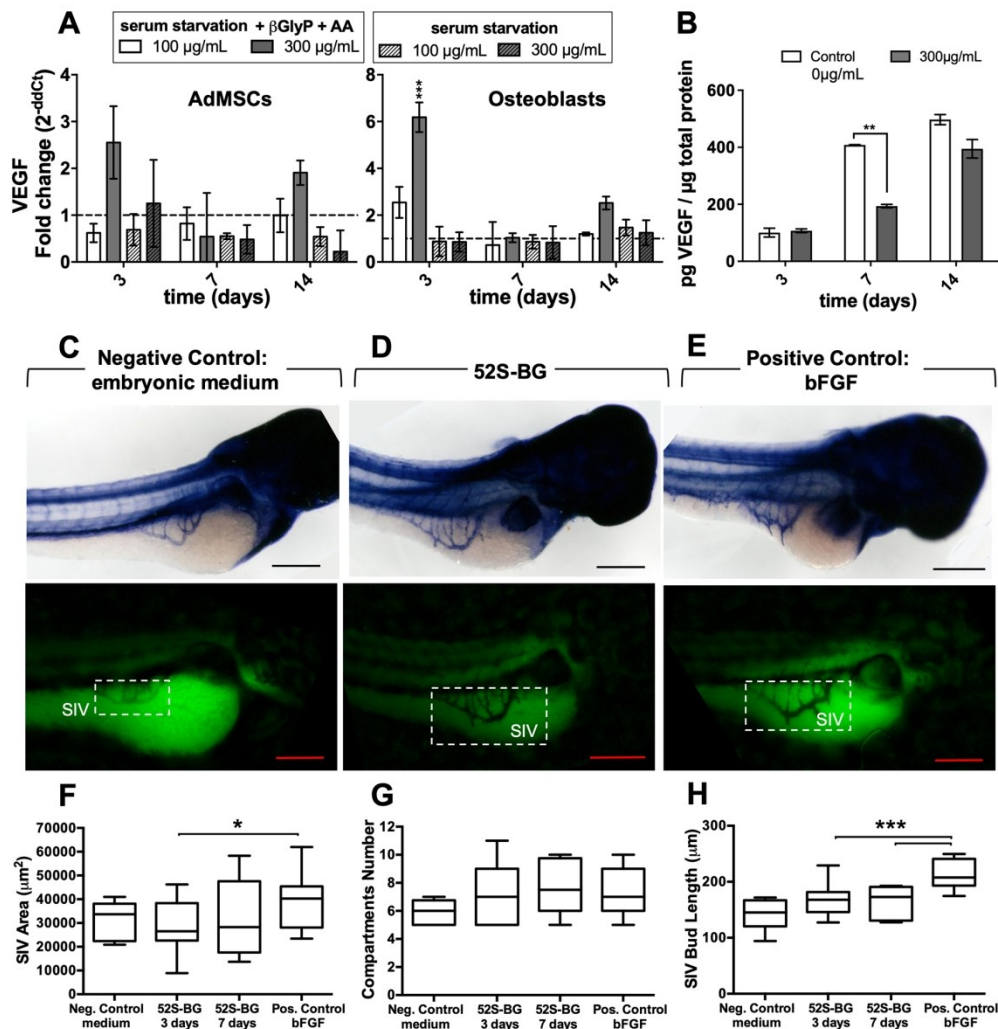


Figure 5. In vitro and in vivo angiogenic properties of the 52S-BG particles. A) VEGF gene expression in human adipose-derived mesenchymal stem cells (AdMSCs) and human osteoblasts (OBs) after culture in the presence of 100 or 300  $\mu$ g/ml 52S-BG particles for 3, 7 or 14 days. The effect of adding  $\beta$ -glycerophosphate ( $\beta$ GlyP) and L-ascorbate-2-phosphate (AA) is shown. Results are expressed as fold change (mean  $\pm$  SEM) of ddCt values ( $2^{-ddCt}$ ) with respect to the control sample (dashed line). \*\*\*  $p < 0.001$ . B) VEGF production by AdMSCs at 3, 7 and 14 days after stimulation with 300  $\mu$ g/ml 52S-BG particles. Results are expressed as pg VEGF normalized to the total protein content (mean  $\pm$  SEM). \*\*  $p < 0.01$ . C) – E) Subintestinal vascular plexus of zebrafish embryos 72 hpf (side view) at 24 h post-stimulation with the ionic dissolution products from the 52S-BG particles. The sub-intestinal vein (SIV) used for semi-quantification purposes is shown within the dashed squares. Representative images are shown for negative control, 52S-BG particles and positive bFGF control. Scale bars = 500  $\mu$ m. Results of the Fiji quantification are presented as a boxplot with whiskers from minimum to maximum: F) SIV area, G) number of compartments per SIV and H) length of the SIV basket. \*  $p < 0.05$  and \*\*\*  $p < 0.001$ .  $n = 60$  individual zebrafish embryos were analyzed per group.

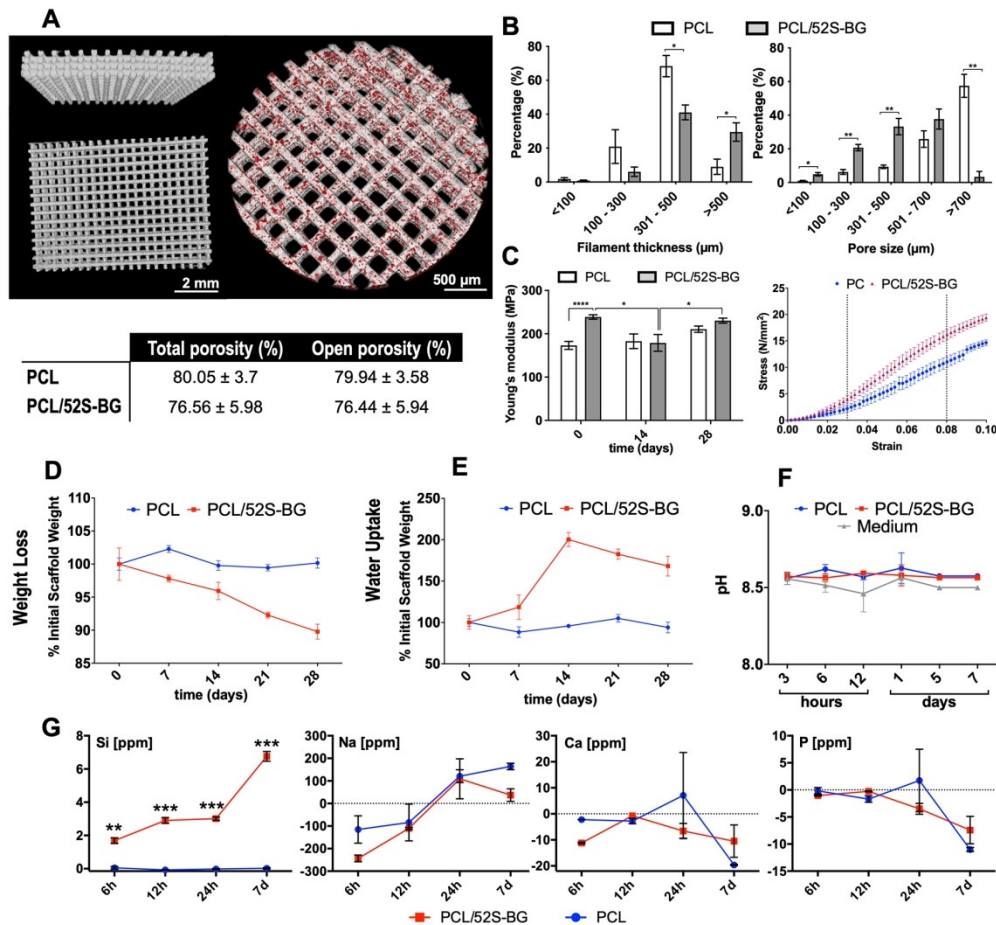


Figure 6. Characterization of PCL/52S-BG composite scaffolds. A) 3D  $\mu$ CT reconstruction image showing the microstructure of the obtained PCL (left side; side and frontal views) and PCL/52S-BG (right side) scaffolds. Red dots, indicating embedded 52S-BG particles, illustrate the distribution of the glass within the PCL matrix (white). Total and open porosity percentage are reported in a table below the images. B) Filament thickness and pore size of the obtained PCL and PCL/52S-BG scaffolds as calculated by  $\mu$ CT ( $n = 6$ ; mean  $\pm$  SEM). C) Mechanical characterization of PCL and PCL/52S-BG scaffolds shown by the Young's modulus (mean  $\pm$  SEM, MPa). Scaffolds were tested before ( $t = 0$  days) and after ( $t = 14$  or  $28$  days) of immersion in PBS. Also depicted are the stress-strain curves obtained for PCL and PCL/52S-BG scaffolds before ( $t = 0$  days) immersion in PBS.  $n = 8$  scaffolds per group were used for the mechanical analysis. D) Weight loss and E) water uptake of PCL and PCL/52S-BG scaffolds upon 28 days of incubation in PBS. Results are expressed as the percentage of either weight loss or weight gain ( $n = 8$ ; mean  $\pm$  SEM). F) pH variation of low glucose DMEM as a result of incubation of PCL or PCL/52S-BG scaffolds for up to 7 days ( $n = 3$ ; mean  $\pm$  SEM). G) Cumulative release of Si, Na, Ca and P ions from PCL and PCL/52S-BG scaffolds upon incubation in low glucose DMEM for up to 7 days. The data were normalized to the DMEM ionic concentration ( $n = 3$ ; mean  $\pm$  SEM). \*  $p < 0.05$ , \*\*  $p < 0.01$ , \*\*\*  $p < 0.001$ , \*\*\*\*  $p < 0.0001$ .

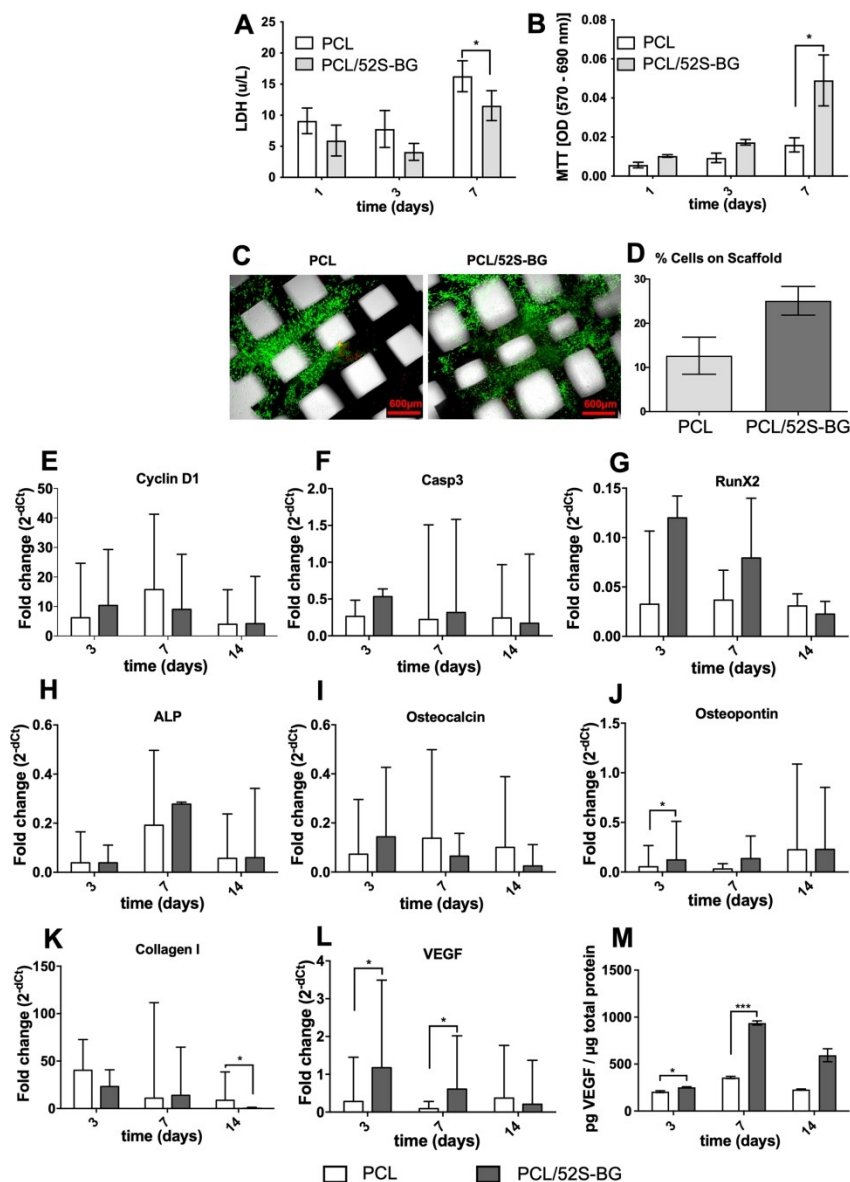


Figure 7. Biocompatibility and gene expression of AdMSCs cultured on PCL/52S-BG composite scaffolds. A) LDH release, B) metabolic activity (MTT test) and C) calcein AM/PI staining analysis performed for AdMSCs cultured on PCL or PCL/52S-BG scaffolds for up to 7 days. Fluorescence microscopy images show viable cells in green and apoptotic cells in red. D) Seeding efficiency of AdMSCs on PCL and PCL/52S-BG scaffolds. The results are expressed as the percentage of cells attached to the scaffold surface at 24 h after seeding with respect to the total cell population. E) – L) Gene expression of the proliferation and apoptosis markers Cyclin D1 and Casp3, respectively, as well as the osteogenic markers RunX2, ALP, osteocalcin, osteopontin and collagen I and the angiogenic marker VEGF. Gene expression is reported as fold change of dCt values (2<sup>-dCt</sup>) with respect to the housekeeping gene  $\beta$ -tubulin. M) VEGF production by AdMSCs cultured on PCL or PCL/52S-BG composite scaffolds. VEGF protein quantification in the cell supernatant was normalized to the total protein content (mean  $\pm$  SEM). \* p < 0.05, \*\*\* p < 0.001, n = 3 scaffolds used for analysis.

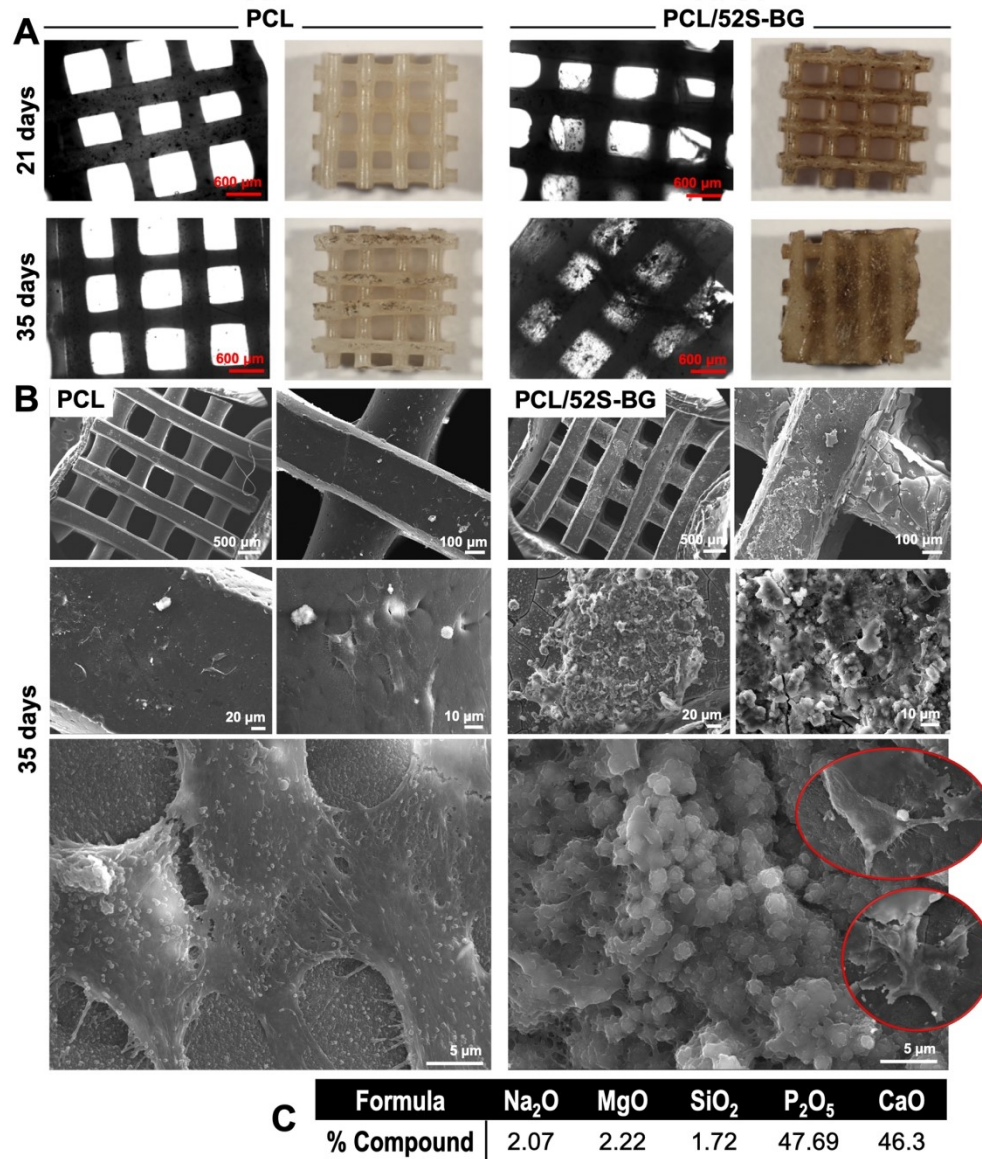


Figure 8. Mineralization of AdMSCs cultured on PCL/52S-BG composite scaffolds. A) von Kossa staining of AdMSCs cultured on PCL and PCL/52S-BG scaffolds for 21 or 35 days. Matrix deposits can be identified occluding the pores of the PCL/52S-BG composite scaffolds. B) SEM images of the AdMSC-seeded scaffolds after 35 days of in vitro culture. Higher magnification images at the bottom of the figure show cells adhered to the scaffold surface as well as cellular matrix deposition. C) EDX semi-quantification of mineral deposits found on the surface of PCL/52S-BG scaffolds.